

NASA Contractor Report 3095

NASA
CR
3095
c.1

TECH LIBRARY KAFB, NM

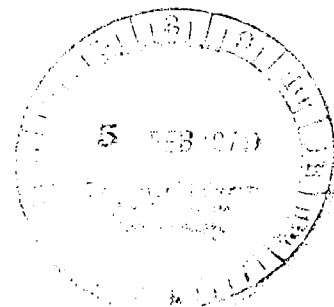
0061879

A Field Study of Air Flow and Turbulent Features of Advection Fog

J. D. Connell

CONTRACT NAS8-32031
JANUARY 1979

NASA





NASA Contractor Report 3095

A Field Study of Air Flow and Turbulent Features of Advection Fog

J. D. Connell
University of Tennessee Space Institute
Tullahoma, Tennessee

Prepared for
George C. Marshall Space Flight Center
under Contract NAS8-32031



National Aeronautics
and Space Administration

**Scientific and Technical
Information Office**

1979

FOREWORD

The work reported herein was supported by the National Aeronautics and Space Administration, Marshall Space Flight Center, Space Sciences Laboratory, Atmospheric Sciences Division, under contract number NAS8-32031.

ACKNOWLEDGMENTS

The author is indebted to Mr. Jack Enders of the Aviation Safety Technology Branch, Office of Advanced Research and Technology (OAST), NASA Headquarters, Washington, D.C., for his support of this research. Special thanks also to Otha H. Vaughan, Jr., of Marshall Space Flight Center, who was the scientific monitor of this research program. Additional support to this research program was provided by Mr. R. McBeth (NCAR, Boulder), Mr. L. Gilchrist (Technician), and three graduate students, Leonard Lally, David Koepf, and Edward Marquart.

TABLE OF CONTENTS

	Page
I. INTRODUCTION	1
II. EQUIPMENT AND INSTRUMENTS	1
A. Basic	1
B. Peripheral Instrumentation	4
C. Planetary Boundary Layer Profiling Balloon System ...	4
III. A PRELIMINARY FIELD TEST AT UTSI	4
A. Wind, Turbulence, and Temperature Measured with the Tower System	6
B. Turbulence Distribution Measured with the Acoustic Radar System	7
IV. A TRIAL FOG MEASUREMENT PROGRAM AT UTSI	15
V. THE ISLAND FIELD LABORATORY	25
A. The Siting of Instruments	25
B. Shelters	25
C. Operational Aspects of the Island Site	25
VI. A FOG CASE STUDY AT THE REMOTE LAKE SITE	29
VII. CONCLUSIONS	30
A. Interpretation of the Measurements	30
B. Recommendations	39
APPENDIX A: DIGITAL COMPUTATION OF THE TURBULENCE PROPERTIES OF THE THREE-DIMENSIONAL AIRFLOW MEASURED WITH A METEOROLOGICAL TOWER	41
APPENDIX B: THE RELATION BETWEEN THE STRENGTH OF ACOUSTIC ECHOES AND PROPERTIES OF TURBULENCE	43

LIST OF ILLUSTRATIONS

Figure	Title	Page
1.	The bistatic acoustic radar components	2
2.	The hotfilm anemometer bridge and probe	3
3.	The 110 V/220 V 60-Hz power generator at the island site	3
4.	Tether-balloon boundary layer profiler (BLP) at the UTSI test site	5
5.	Instrumented test site at UTSI	5
6.	Closeup of test site at UTSI, showing the lake behind the slant-beam acoustic antenna	6
7.	An oblique view from above the UTSI test site showing the spatial arrangement of the equipment	8
8.	Acoustic radar monostatic echoes up to 350 m above the ground and horizontal wind and turbulence at 12 m above the ground	10
9.	A comparison between the acoustic radar chart record and a detailed oscilloscope display of the same echo-voltage versus time at four heights selected from the chart	12
10.	Alternating half-hour segments of acoustic radar monostatic (M) echo and bistatic (B) echo up to 1 km above the ground prior to and at onset of thunderstorm	13
11.	Continuation of the acoustic radar record started in Figure 10	14
12.	Vertical distribution of temperature measured by thermocouple junctions on the meteorological tower on 26 March 1977	16

LIST OF ILLUSTRATIONS (Concluded)

Figure	Title	Page
13.	Acoustic radar and wind data just prior to formation of fog	17
14.	Daily variation of surface atmospheric temperature (a) and relative humidity (b) and static pressure (c) from 22 to 28 March 1977	19
15.	Meteorological tower data, 1231 to 1243 LST 22 March 1977, on the day before fog formed	21
16.	Meteorological tower data, 1315 to 1325 LST 23 March 1977	22
17.	An oblique drawing of the island and instrumentation setup	26
18.	A telephotographic view (toward the northwest) of the island site (on the left) and the University of Tennessee Space Institute across the lake (on the right)	27
19.	A close telephotographic view of some of the instrumentation and shelters on the island	27
20.	An outline map of the lake, the island field site, and the UTSI laboratory site	28
21.	Sample acoustic radar record taken at the island site during fog	31
22.	Sample vertical distributions of atmospheric boundary layer temperature, wet-bulb temperature, horizontal wind speed, and horizontal wind direction measured from a tethered-balloon boundary layer profiler	33
23.	Smoothed graphs of atmospheric variables at the surface at the island site during the time interval which includes the dissipation of a fog	38
24.	A fog bank northwest of the island site	40

A FIELD STUDY OF AIR FLOW AND TURBULENT FEATURES OF ADVECTION FOG

I. INTRODUCTION

This research program was undertaken to provide data relative to the air flow and turbulence features of warm fog forming due to advection conditions at a lake site. Data from this research are also being used to refine computer models which are being developed to understand the life cycle characteristics of fog formation. It is hoped that, by a thorough understanding of fog formation and dissipation, data will evolve to allow better techniques to be developed for modification of dense fogs at airports.

Dense fogs at airports create considerable hazards and impair safe and efficient operations of aircraft and movement of passengers. Fogs at airports are responsible for revenue losses of approximately \$100 million annually (estimated by the Airline Transport Association) because of air carrier flight cancellations, diversions, and delays. In addition, a considerable number of persons are injured or killed each year in fog-related accidents in commercial and general aviation operations.

The various pieces of equipment used at the lake site and the results of the data obtained are discussed in the following sections.

II. EQUIPMENT AND INSTRUMENTS

A. Basic

The fundamental tool for the field study is the monostatic-bistatic acoustic radar. A standard commercial model was used because of its availability, relatively wide use, and portability and because it reputedly operates well even when powered by automobile batteries and a small inverter available through the same vendor. Figure 1 contains drawings and a photograph of the main components of the acoustic radar system.

Several hotfilm anemometers were evaluated for making measurements in the two-phase flow of warm fog. A standard research grade constant-temperature model made in the U.S. was chosen. The hotfilms were 20 μ in

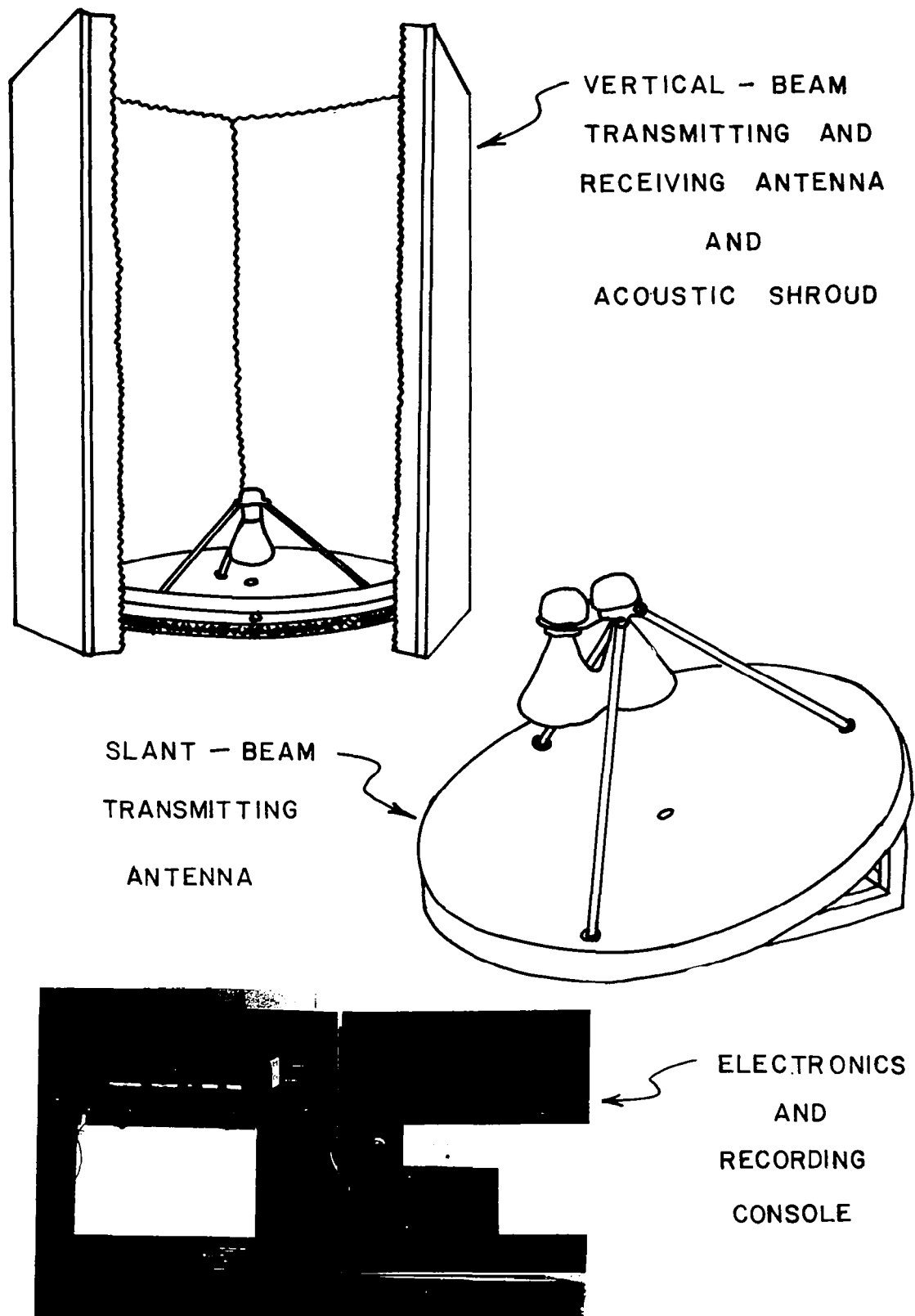


Figure 1. The bistatic acoustic radar components.

diameter, and one of the two probes was constructed for use in liquid water but calibrated in air. Figure 2 contains a photograph of the anemometer console and the probe.

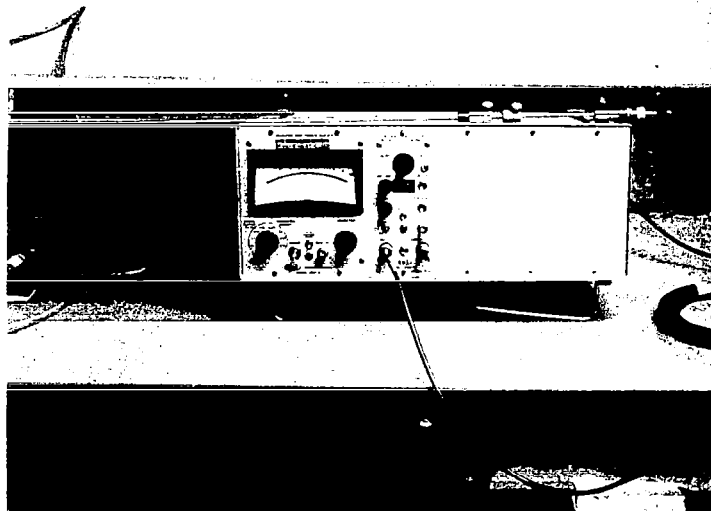


Figure 2. The hotfilm anemometer bridge and probe.

It became clear that the automobile battery-inverter system would not be adequate for the instrumentation at the remote site. Therefore, a standard 4-kW, 110 V/220 V, 60-Hz gasoline-powered contractor model generator was purchased together with an auxiliary 20-gal gasoline tank. Figure 3 presents the generator at the field site.

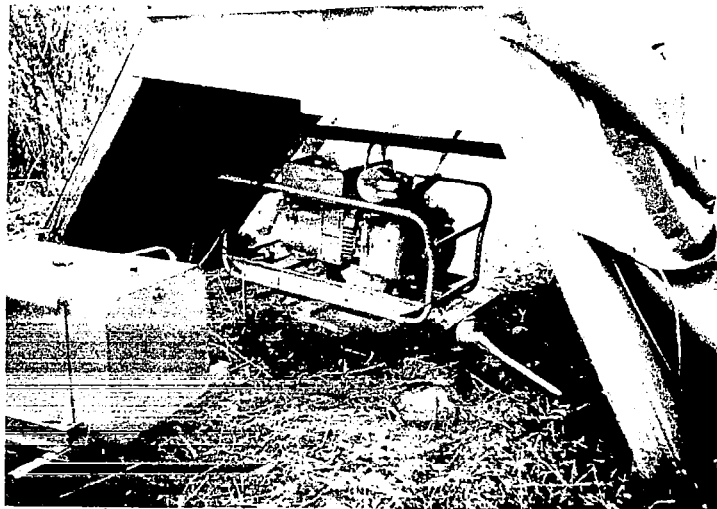


Figure 3. The 110 V/220 V 60-Hz power generator at the island site.

B. Peripheral Instrumentation

NASA provided a 10-m tower and instrumentation. To mount the tower securely on a base at water level on the shore of an island, it was necessary to drive pilings upon which a platform was constructed. Special guy wire tie points were placed in the ground under the water.

Five transmissometer systems were also used to collect visibility data. Three systems were functional in the controlled environment of a laboratory. One was operated briefly in the field fog environment.

A standard U.S. model hygrothermograph and a microbarograph were used, and a standard surface station shelter contained the instruments at a shoreline site well exposed to the lake airflow.

Copper-constantan thermocouple wire and a six-channel, chart-recording potentiometer and mercury thermometers were used for measuring an absolute reference temperature of the lake water.

C. Planetary Boundary Layer Profiling Balloon System

The tethered balloon, measurement and telemetering package, recorder, winch, and baseline check instruments were provided by the Field Observation Facility of the National Center for Atmospheric Research (NCAR). The balloon system being deployed for training purposes at the University of Tennessee Space Institute (UTSI) laboratory (not the lake site) is shown in Figure 4.

The system described previously comprises the instrumentation used for the first fog measurements at the island site. However, several modifications are desirable based upon results discussed in the remaining sections of this report.

III. A PRELIMINARY FIELD TEST AT UTSI

Because travel to the over-water field site was difficult and neither continuous electrical power nor all test equipment could be provided there, a preliminary site was set up at UTSI. This provided an excellent site for operation of the acoustic radar system. Figure 5 shows the white acoustic shroud for the vertical-beam antenna of the radar. The shroud for the slant beam antenna is



Figure 4. Tether-balloon boundary layer profiler (BLP)
at the UTSI test site.



Figure 5. Instrumented test site at UTSI.

the box-like structure just left of the short (10-m) tower. The fog study instrumentation trailer is behind the tall (20-m), permanent meteorological tower. This site is on a peninsula on the north shore of Woods Reservoir. The lake can be seen beyond the gap in the trees. Figure 6 presents a closeup of the lake. The slant-beam acoustic antenna has been removed from its shroud. It is the dish-like object in the middle of the photograph.

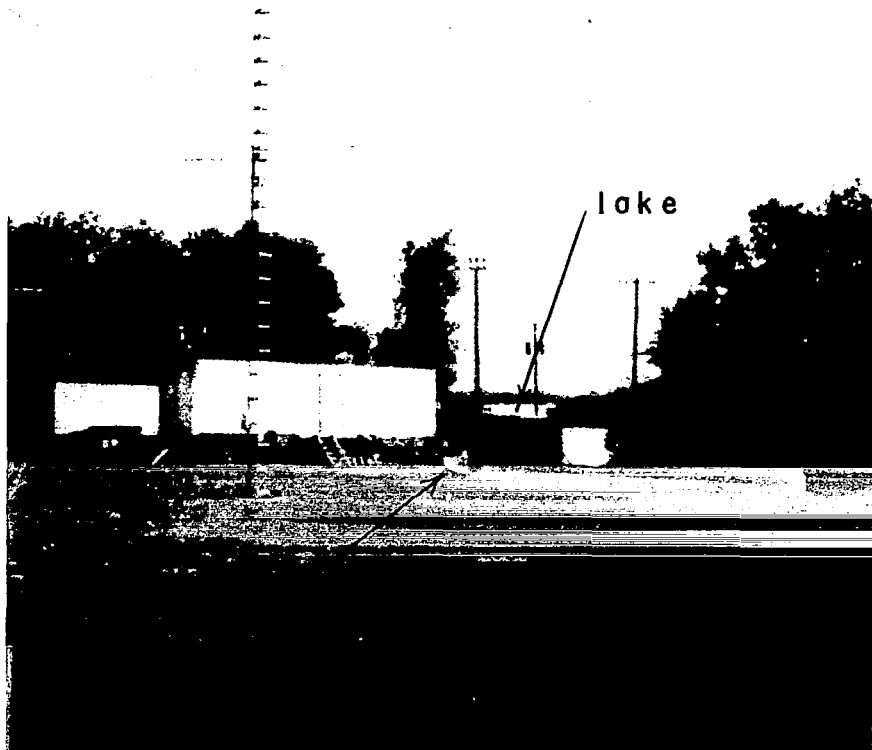


Figure 6. Closeup of test site at UTSI, showing the lake behind the slant-beam acoustic antenna.

A. Wind, Turbulence, and Temperature Measured with the Tower System

A continuous paper chart record of the three-dimensional wind velocity at the 12-m height and the horizontal wind speed at the 21-m height is made at a chart speed of 5.08 cm (2 in.)/hr and with adequate resolution in wind speed and direction. For selected periods where detailed structure of the atmosphere was required the chart speed was set at 5.08 cm (2 in.)/min. The temperature

increment between four heights (0.5, 1, 2 and 12 m) on the tower was recorded with 0.1°C resolution at a chart speed of about 0.5 cm/min. The thermocouple junction at the 2-m level was used as a reference (in air).

B. Turbulence Distribution Measured with the Acoustic Radar System

During the test period at the UTSI site, the radar detected atmospheric turbulence effects for many different synoptic and local conditions. The resulting continuous record of the echo structure in the boundary layer was used as a basis for evaluating the usefulness of the radar. Further, the series of echo records provided a local reference against which to compare acoustic echoes associated with local fog conditions.

Several examples of the echo patterns recorded at UTSI are included in the present section. One of the examples is of a cold-advection fog.

The configuration of instrumentation at the laboratory site is shown by the oblique-view drawing in Figure 7.

The acoustic radar, an Aerovironment Model 300 system coupled to a slant-beam second sending antenna, made possible the options of observing the backscatter of sound pulses from thermally turbulent regions in the planetary boundary layer or observing the scatter at 135 to 150 degrees from the forward direction from regions having velocity and temperature fluctuation.

The echo analysis and display scheme used with the acoustic radar does not provide direct records of wind speed, although speed information is in the echo. The present model of acoustic radar measures distances to the scattering volumes and, more inexactly but quite usefully, the intensity of the fluctuations from which the scattering occurs.

The backscatter echoes come from regions where the speed of sound varies strongly due to temperature variations. The temperature variation usually is due to turbulence at inversions or in thermals. The sensing of the velocity fluctuations of turbulence occurs only at angles of scatter different from 180 degrees. When there are weak temperature fluctuations in small (20-cm diameter) volumes and consequently no backscatter from existing turbulence is detected, the turbulence may be observed using a slant beam which can be scattered into the receiving antenna.

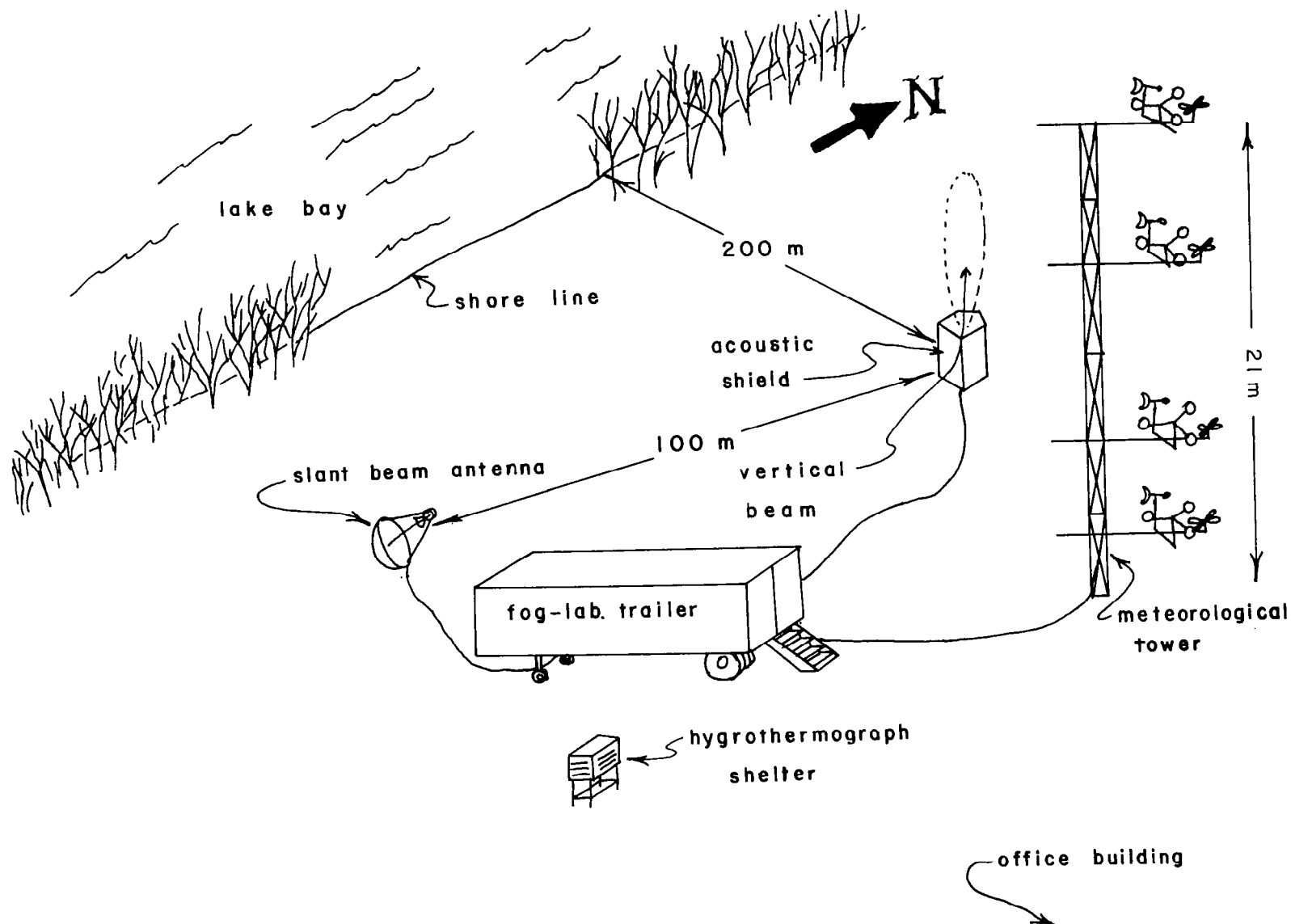


Figure 7. An oblique view from above the UTSI test site showing the spatial arrangement of the equipment.

The recorded intensity of acoustic echo is related to the turbulence intensity. Figure 8 contains the backscattering record for a fairly strong inversion at night from 2100 local standard time (LST) 25 March 1977 to 0500 LST 26 March 1977. The acoustic radar record is at the bottom of the figure. The time scale in days and hours is at the top and bottom of the figure. The echo strength plotted includes a correction for the $(\text{range})^{-2}$ loss due to spreading of the sound energy scattered. Thus, the plot gives an estimate of the vertical distribution of the structure coefficient of temperature fluctuations, C_T . It is associated mostly with turbulence (velocity fluctuation) which is bounded by strong mean temperature differences such as occur at inversions or in buoyant plumes.

The structure coefficient is given in terms of temperature fluctuation at two points as follows:

$$C_T = \frac{\overline{T'(x) - T'(x+r)}}{r^{2/3}}$$

where

T' = the difference between the actual temperature at time t and the time average temperature

x = the position along the acoustic ray path

r = the separation distance along x between points at which T is to be measured.

The overbars indicate ensemble averages or long time averages.

The acoustic radar as conventionally set up cannot observe the lowest 25 m of the atmosphere because of its inherent "dead time." The 15-m thick band starting at $Z = 0$, the initial pulse, is followed by a 10-m thick white (dead time) band. Atmospheric echo is recorded above the white band. The intense turbulence in the layer from 25 m to between 60 and 120 m heights may not have its structure resolved because the dynamic range of echo intensity of the chart recording system is not great enough. At lesser intensities of turbulence there is a broader range of intensity resolution possible and interesting multiple layers of the inversion are displayed. The individual laminae are mostly no greater than 20 to 30 m thick vertically. Some features appear to be 50 to 100 m thick.

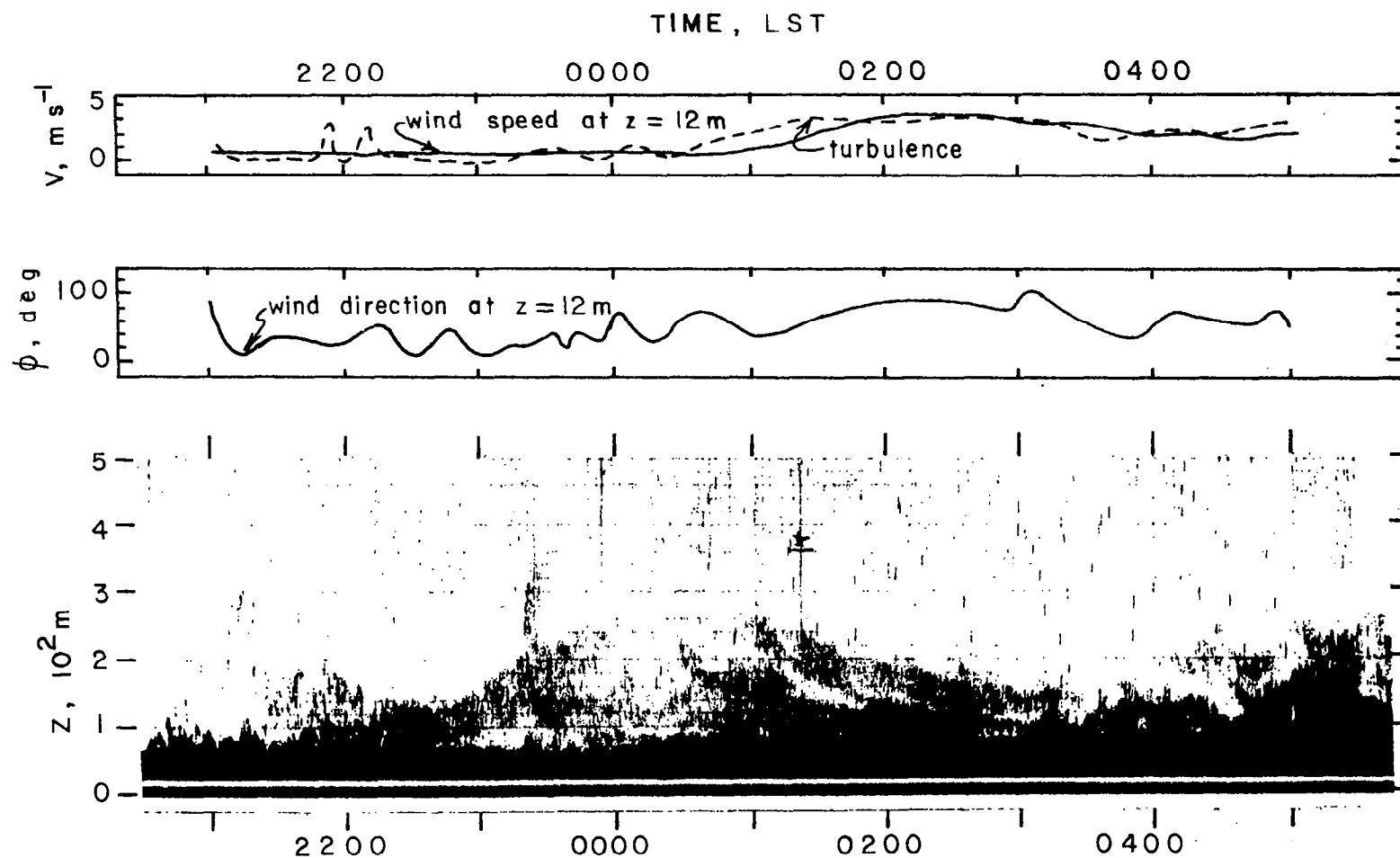


Figure 8. Acoustic radar monostatic echoes up to 350 m above the ground and horizontal wind and turbulence at 12 m above the ground (Time: 2100 LST 25 March 1977 to 0500 LST 26 March 1977).

Variations in height of turbulent layers at a rate of 100 m hr^{-1} , such as shown between 0400 and 0530 LST causing 150-m height increases and decreases, are probably due to gravity waves. The echo height, number of echo zones, and total thickness of the turbulence-filled zones between thermally stratified layers vary strongly and somewhat regularly. The paper chart record can be used for quantitative time and space analysis and for qualitative C_T and turbulence intensity analysis. The signal received could be treated more quantitatively if recorded as a coordinate on a chart, as a voltage on magnetic tape, or as a dot matrix printed on paper. Figure 9 shows an oscilloscope display of height versus acoustic echo signal amplitude. The full dynamic range of the echo may be retained by variations of this method, but it does not lend itself to easy presentation of a large series of sequential soundings.

It is possible to use a second antenna as the sound emitter and to select an angle of scatter to the first antenna such that temperature fluctuations and velocity fluctuations are observed. Then the scattered intensity at the selected angle is a measure of a weighted sum of the velocity structure coefficient, C_V , and C_T . Unless the Doppler shift information in an echo is used to directly measure velocity variation, the bistatic radar detection of C_V is the most direct method of describing the turbulence field. Sometimes the ratio of turbulence intensity to temperature gradient is so great that the temperature fluctuations are mixed to very low values and the monostatic method of estimating turbulence distributions through C_T distributions is not functional. An example of such an atmospheric condition is shown in the acoustic radar record of Figure 10, taken on a thunderstorm day. Figure 11 continued the record which is described briefly in the next paragraphs.

The time increases from left to right at approximately 1 hr/in. The time interval of the record is from approximately 0200 to 1800 LST on 28 March 1977. The sky was overcast by middle-level cloud at least. The acoustic radar was run in the alternating mode with half-hour intervals each of monostatic (M) and bistatic (B) operation. The left one-third of the record is from 3 hr before dawn to 3 hr after dawn. The dark portions of the record which extend down from the top, or 1000 m position on the chart, are due to wind and light rain. The monostatic records in the left one-third of the record indicate turbulence mostly below the 100-m height. The bistatic records show that there was a very turbulent layer above the 120-m height. It should be pointed out that the bistatic transmitted beam, which is tilted and fanned wide, intersects the receiving volume of the vertical beam between 120 to 360 m above the ground. Thus, as presently positioned, it gives no information for heights below 120 m or above 360 m.

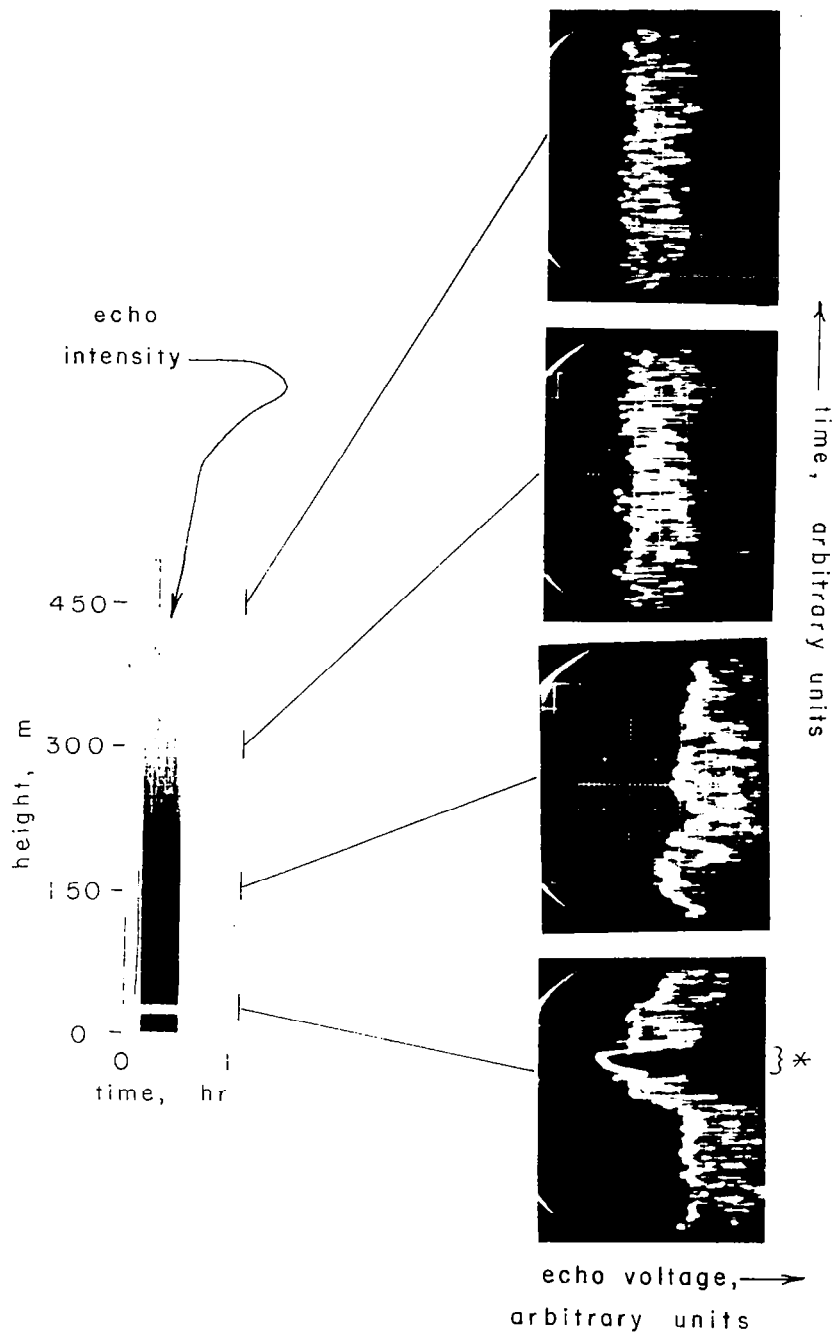


Figure 9. A comparison between the acoustic radar chart record (left side of figure) and a detailed oscilloscope display of the same echo-voltage versus time at four heights selected from the chart (The programmed decrease in voltage marked by an asterisk in the lower right photo of oscilloscope trace eliminates antenna ringing noise which continues briefly after the desired sound pulse is emitted.).

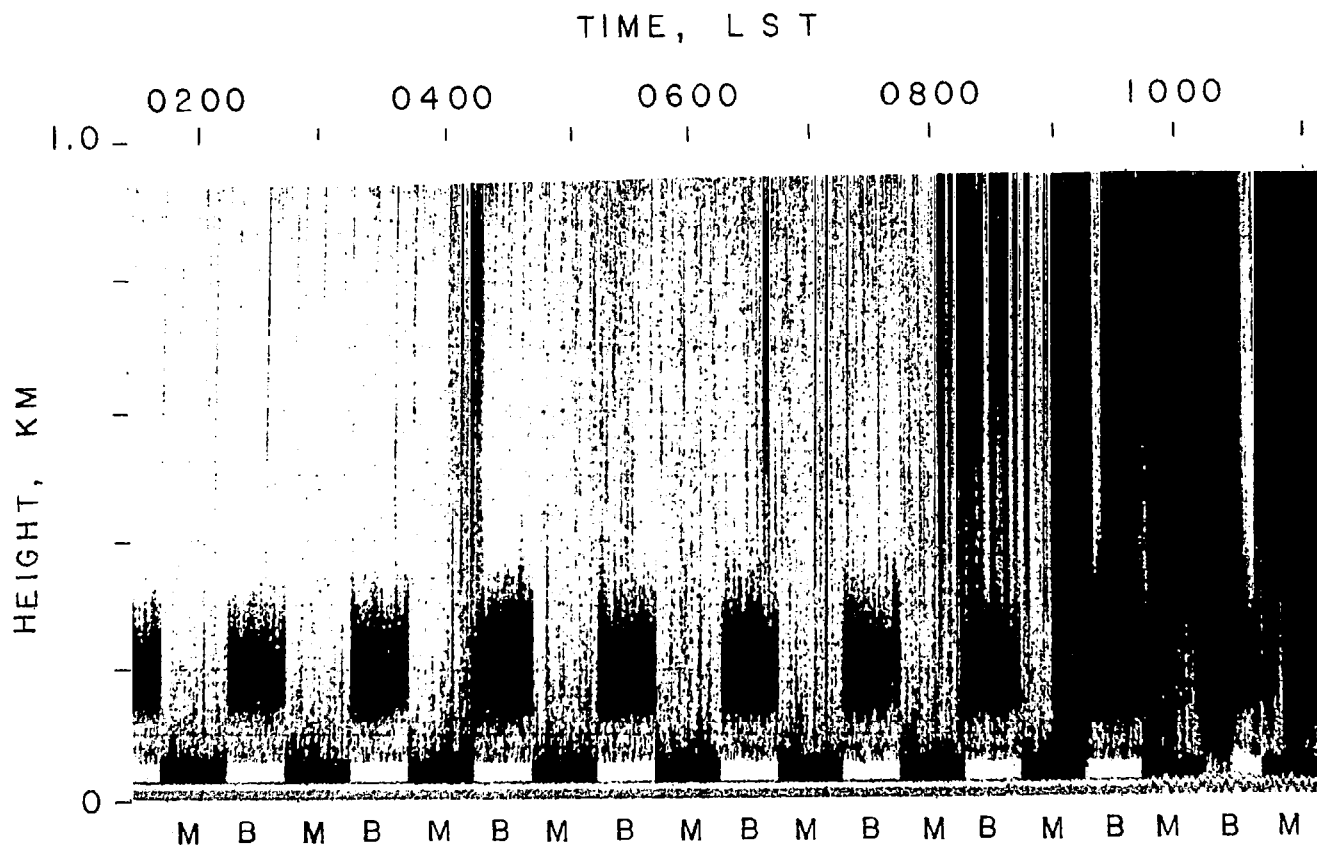


Figure 10. Alternating half-hour segments of acoustic radar monostatic (M) echo and bistatic (B) echo up to 1 km above the ground prior to and at onset of thunderstorm (Time: 0200 LST to 1100 LST, 28 March 1977. Rain shows as black regions extending from the top of the record.).

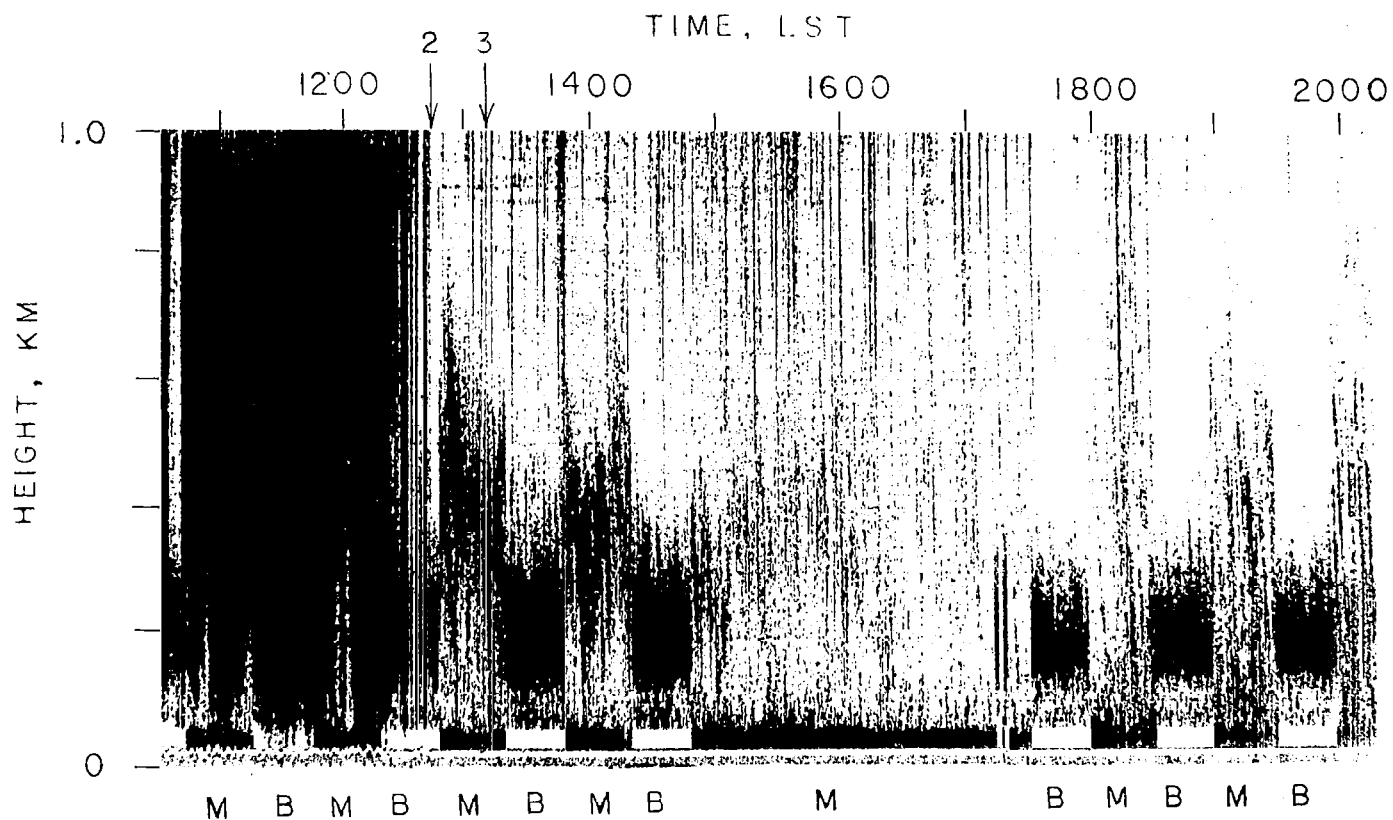


Figure 11. Continuation of the acoustic radar record started in Figure 10. (Arrow 2 indicates the time at which rain ends. Arrow 3 indicates the time of arrival of visible cloud waves, vortices, and turbulence in middle tropospheric levels. The monostatic echoes after this time may be due to evaporating rain aloft.).

In the middle section it is seen that, except for records in the altitude range 25 to 70 m, the acoustic radar record is obliterated by noise from strong wind and rain. Several new features appear in the right-hand one-third of the record. The rain stopped, but some wind noise remained. The thermal fluctuations seem to have had two causes as indicated by the monostatic (M) records. A layer descended from approximately 800 to 400 m in 2 hr at an average speed of 6 cm s^{-1} . The layer was approximately 600-m thick initially and was approximately 200-m thick just before it lifted and disappeared in complex thunderstorm winds. (Waves and vortices were seen in clouds approximately 1 km above ground level). At approximately 1800 LST some stronger thermals seemed to be rising from the lowest 60 m to approximately the 200 m height.

To repeat, the bistatic mode was required to detect the turbulence above the first 60 to 80 m during part of the day.

The preliminary checkout of systems indicated that the acoustic radar, hotfilm anemometer, and tower anemometry were functional and sufficiently accurate for purposes of the present fog study.

Figure 12 contains a profile of temperature, $T(z)$, near the ground derived from thermocouple junctions at 0.5, 1, 2, and 12 m heights on the meteorological tower near the fog laboratory trailer just after sunrise on 26 March 1977. The thermocouple data show a mean lapse rate of $\partial T / \partial Z \doteq -2\text{c}/10\text{m}$ which is very stable. Peak-to-peak fluctuations of temperature for frequencies less than 0.5 Hz were approximately 1°C at $Z = 12 \text{ m}$. The acoustic radar record showed strong multiple inversion with gravity waves near the time of sunrise.

IV. A TRIAL FOG MEASUREMENT PROGRAM AT UTSI

A local fog formed over the bay 200 m west of the fog laboratory trailer sometime during the night of 22-23 March 1977. It lasted until 0700 on 23 March. Cold air advected over warm water, forming moderately dense fog to a depth of approximately 80 m above the lake. The data taken were as follows:

- 1) Acoustic radar monostatic (and bistatic) chart records for $Z = 25 \text{ m}$ (120 m) to 1000 m (360 m) (Fig. 13).

- 2) Microbarograph and hygrothermograph chart records at a rate of approximately 2 in. day^{-1} (Fig. 14).

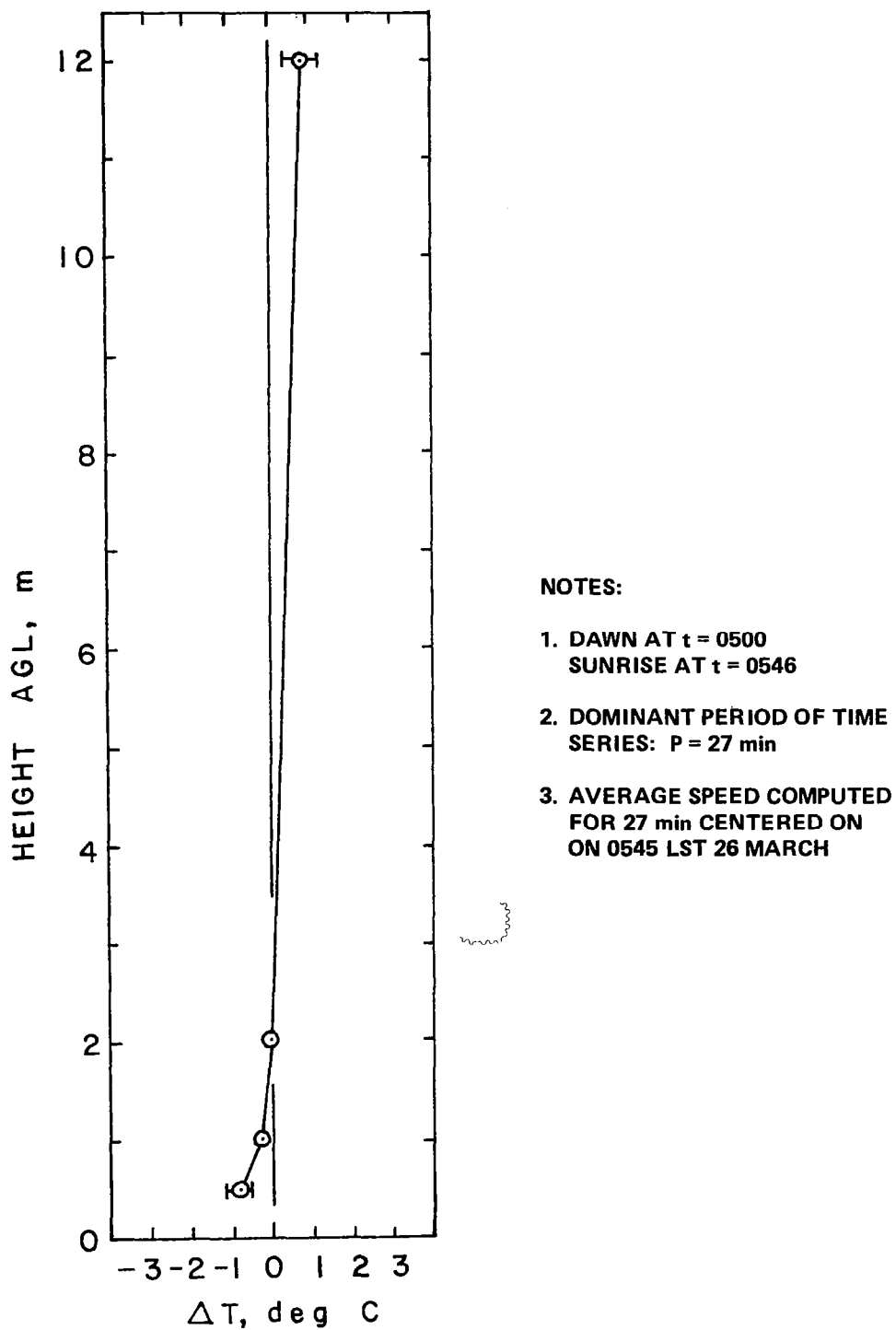


Figure 12. Vertical distribution of temperature measured by thermocouple junctions on the meteorological tower on 26 March 1977. (Both 27-min means and peak-to-peak fluctuations are plotted.)

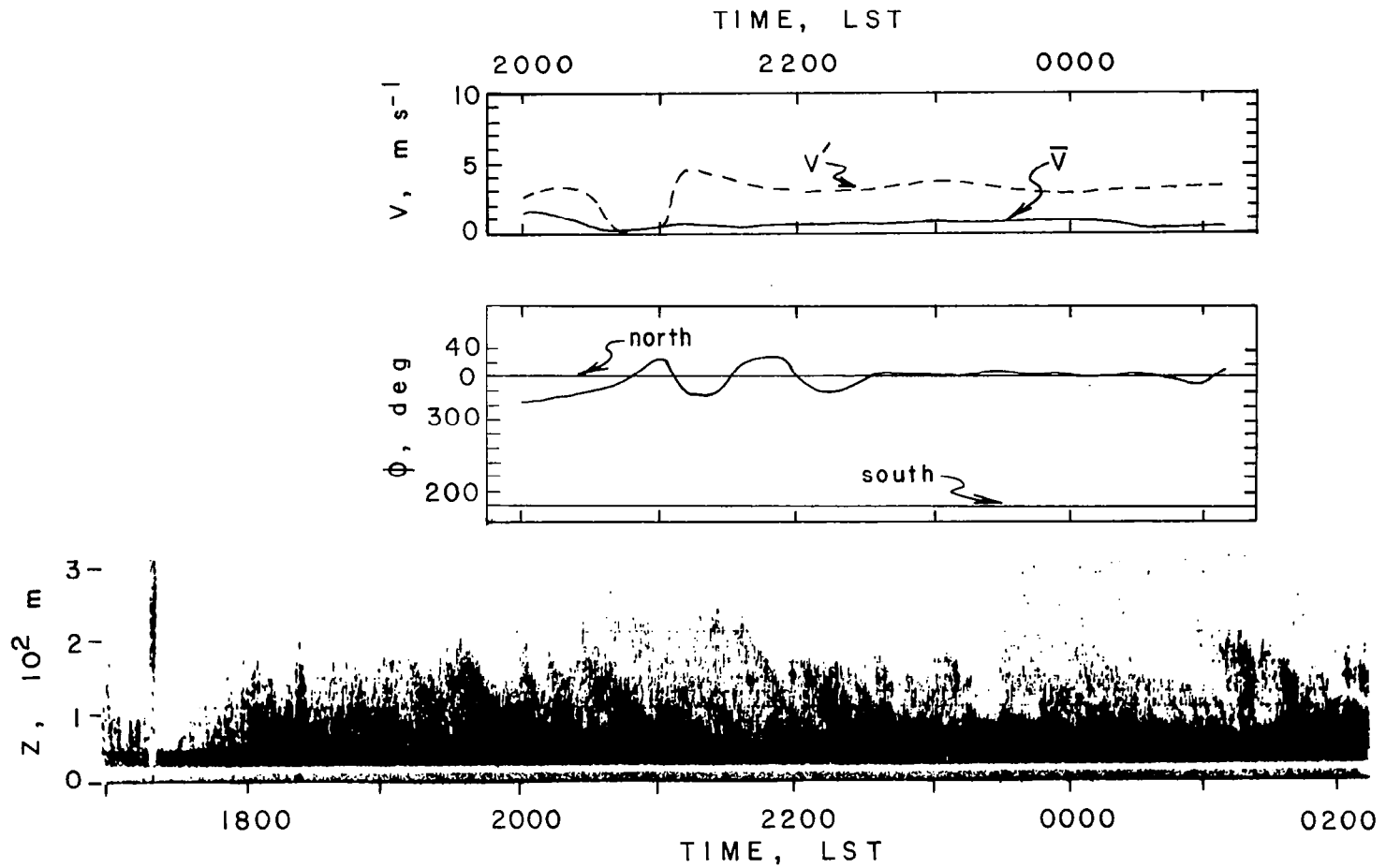


Figure 13a. Acoustic radar and wind data just prior to formation of fog. (Time: 2000 LST 22 March 1977 to 0100 23 March 1977. The upper graph shows running-mean wind speed (solid line) and peak-to-peak turbulence speed (dashed line) at $Z = 12 \text{ m}$. The lower graph shows the time height distribution of monostatic radar echo strength.)

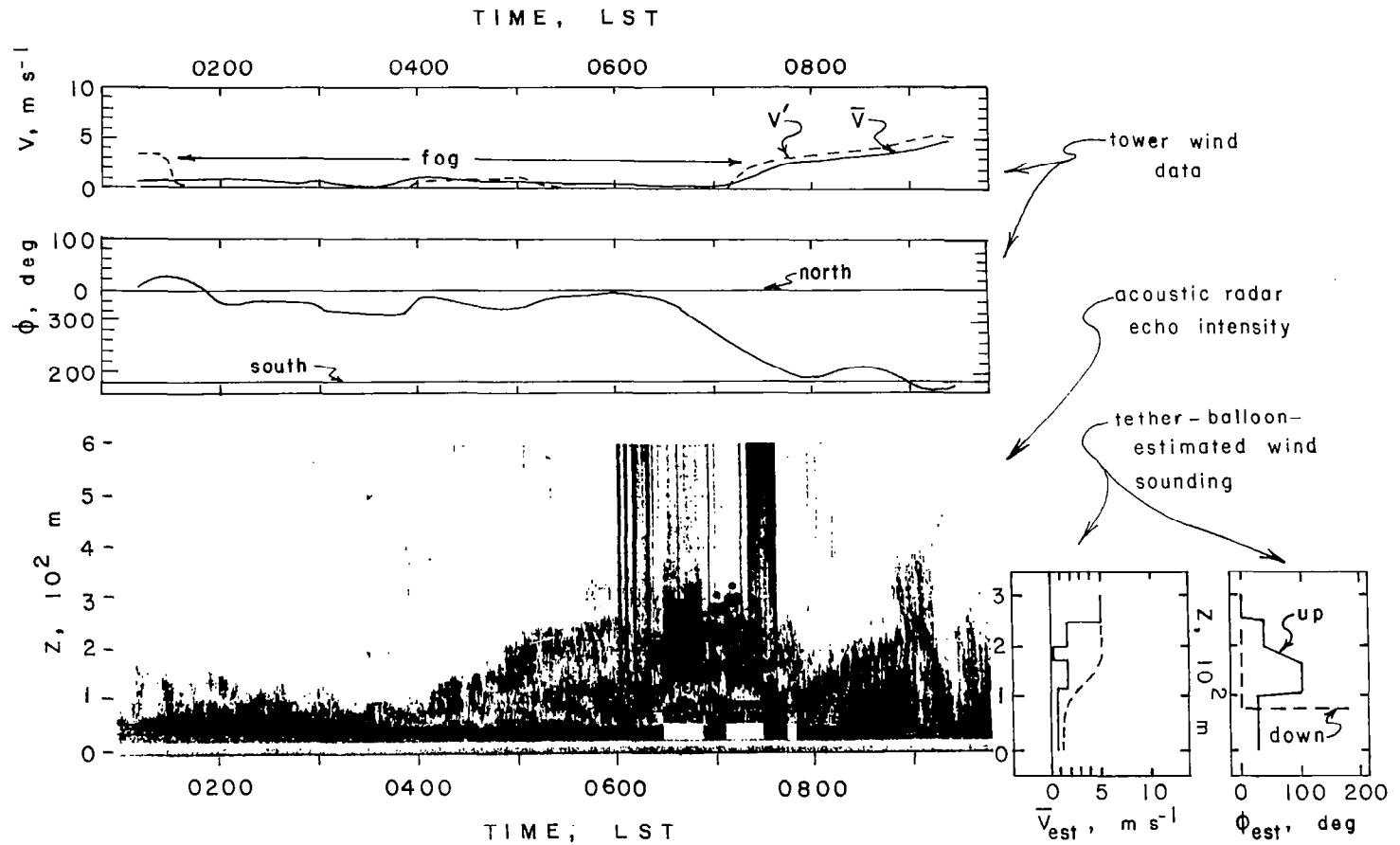


Figure 13b. Continuation of the data time series from Figure 13a. (Fog formed and dissipated during this interval. Time: 0100 LST to 0900 LST 23 March 1977.)

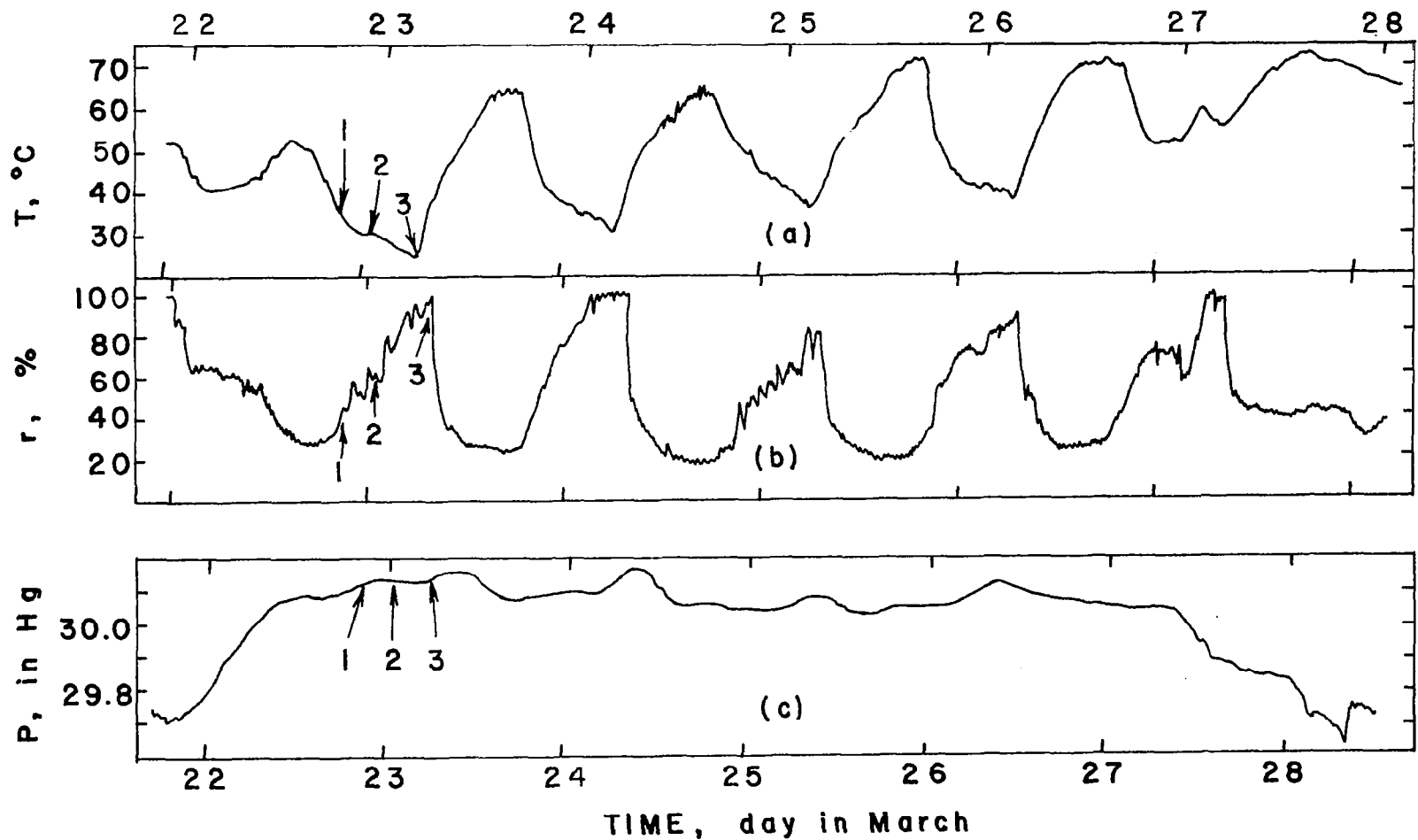


Figure 14. Daily variation of surface atmospheric temperature (a) and relative humidity (b) and static pressure (c) from 22 to 28 March 1977. (Arrows indicate times of (1) wind speed decreases to less than 1 m s^{-1} , (2) turbulence decreases to less than wind speed and 0.1 m s^{-1} , and (3) fog dissipation.)

3) Horizontal wind speed and direction at $Z = 12$ m above the ground at a chart rate of 2 in. hr^{-1} (Fig. 13a upper graphs).

4) Estimates of horizontal wind velocity as a function of height up to $Z = 300$ m above the ground from 0600 to 0730 LST were measured using a tethered helium-filled Jimsphere balloon (Fig. 13b inset).

5) Three-dimensional wind velocity at $Z = 12$ m, plus wind speed at $Z = 21$ m, for the afternoon preceding and the morning following the fog at a chart speed fast enough to permit analysis of the structure of the turbulence (Figs. 15 and 16).

The acoustic radar record and the wind mean velocity and turbulence magnitude at $Z = 12$ m are plotted on the same time scale in Figure 13.

Throughout the previous evening, 22 March, the inversion was below $Z = 200$ m above ground level (Fig. 13a). The average wind direction was from 0 deg, and its variation seemed to reflect the oscillation of a gravity wave at the top of the inversion. Interestingly, the peak-to-peak magnitude of the fluctuations of wind remained at approximately 3 to 4 m s^{-1} until approximately 0130 LST of 23 March (Fig. 13b). At that time the turbulence at the tower decreased to less than 0.2 m s^{-1} , thus for the first time being less than the mean speed. The buoyant convection over the bay would have caused additional turbulence not measured at the tower. It is probable that this decrease of mechanical turbulence may have coincided with the onset of fog, but no transmissometer was functional to measure the existence of fog. Concurrent with the rapid decrease in turbulence at $Z = 12$ m, an acoustic echo began at $Z = 400$ m. It became more intense and thickened to approximately 100 m as it moved downward at approximately 25 m hr^{-1} until approximately 0700, 23 March. At 0700 the top of the layer, which had been thickening upward from the surface since about an hour before dawn, converged with the upper layer. It was at this time that the fog disappeared. The wind speed and turbulence also increased rapidly at this time, and the wind direction became northwesterly and changing toward southerly at the $Z = 12$ m height.

The probable fog interval is indicated on the top graph of Figure 13b. A hypothesis concerning the onset and the end of fog will be deferred until more observations are obtained for fog life interval, intensity, turbulence, and depth.

It is evident that it is important to establish a site in the middle of the lake. However, much can be learned on the shore even at a crosswind site adjacent to the fog.

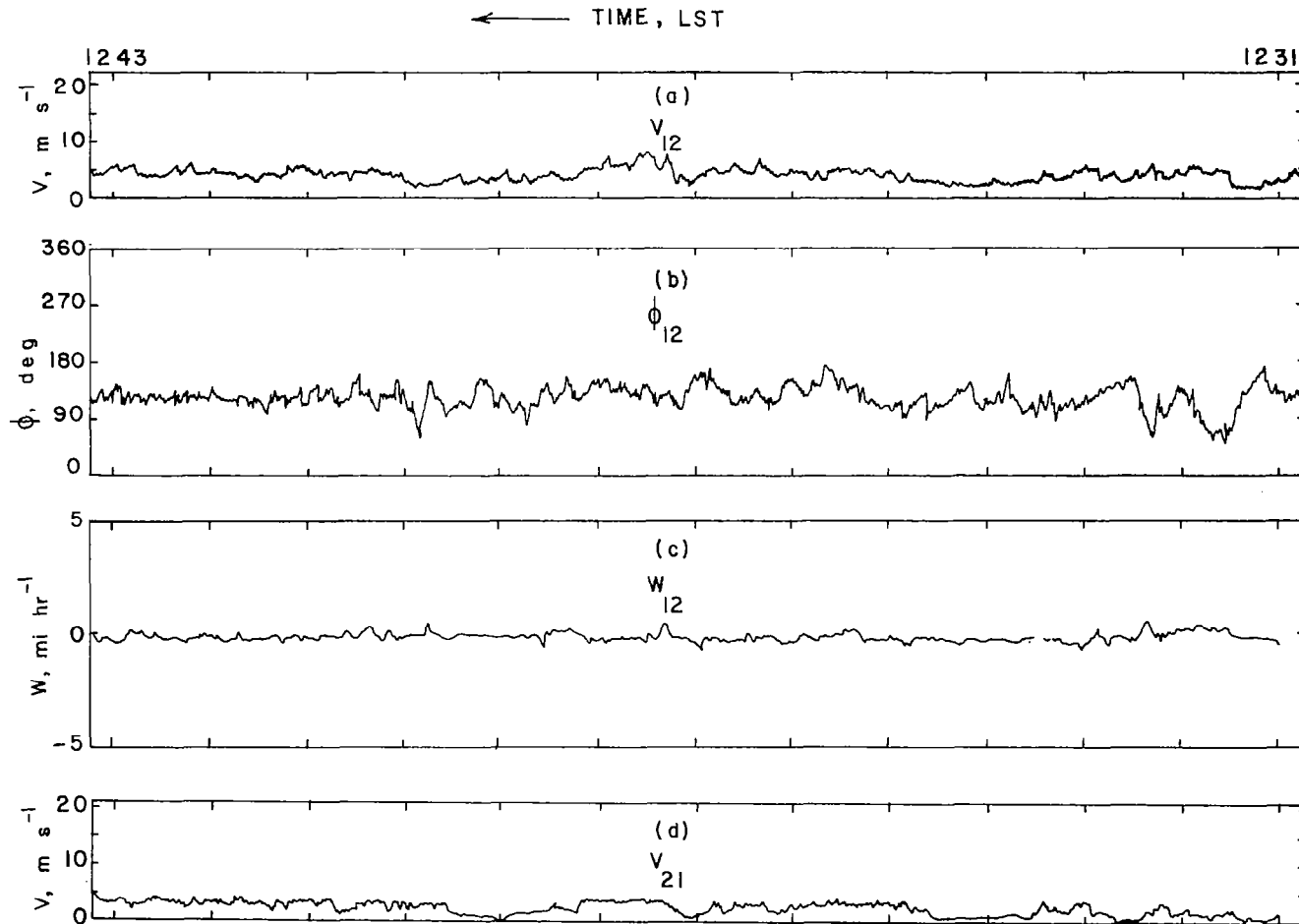


Figure 15. Meteorological tower data, 1231 to 1243 LST 22 March 1977, on the day before fog formed. (Clear skies, synoptic-scale subsidence and strong dry thermals. (a) Horizontal wind speed, (b) direction, (c) vertical wind speed at $Z = 12$ m, and (d) horizontal wind speed at $Z = 21$ m.)

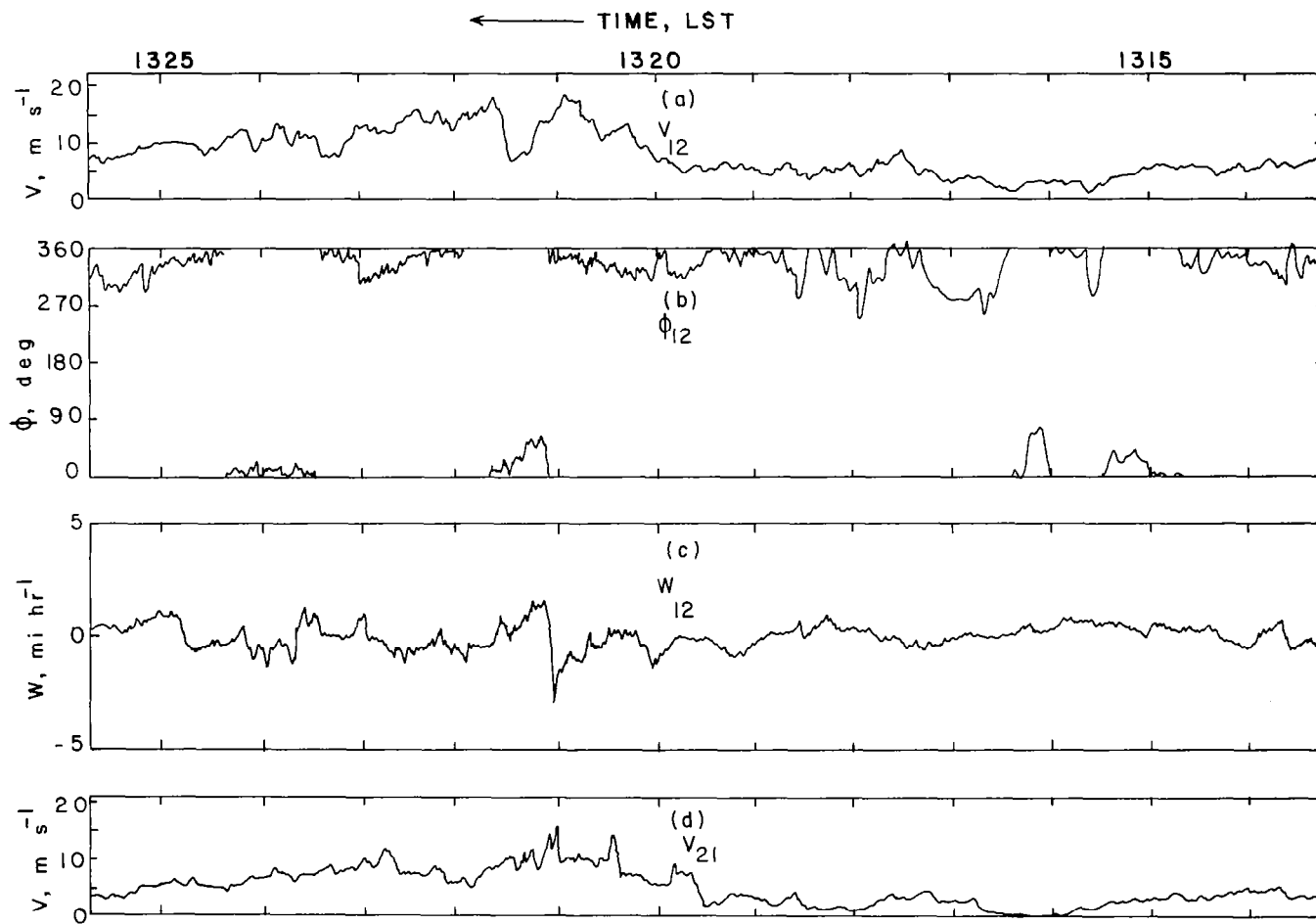


Figure 16. Meteorological tower data, 1315 to 1325 LST 23 March 1977. (Clear skies, synoptic-scale subsidence and moderate dry thermals. (a) Horizontal wind speed, (b) direction, (c) vertical wind speed at $Z = 12$ m, and (d) wind speed at $Z = 21$ m.)

The tethered balloon was let up manually. The echoes from the balloon on the right-hand end of the acoustic radar record have been marked by the small solid dots on the acoustic echo plot in Figure 13b. The heights of the balloon and the direct observations of string directions, shape, and balloon pull were used to estimate the wind velocity profiles plotted in the graphs on the right side (Fig. 13b). The number and location of balloon-measured wind shears are fairly consistent with the acoustic radar echo record, considering the crudeness of the balloon measurements. The complexity of the airflow and turbulence in the first 300 m above the ground is indicated. The value of some temperature and wind measurement apparatus such as a tethered balloon which can make rapid profiles in the first few hundred meters above the ground is that it permits one to make less ambiguous interpretations of the acoustic sounder records.

Figure 14 (a) and (b) shows the diurnal variations of dry-bulb temperature and relative humidity. Clearly, the morning of the fog had the lowest minimum temperature (by 5°C) for the week. The times of onset of wind speed below 1 m s^{-1} and turbulence to less than 0.1 m s^{-1} are marked, as is the time of dissolution of the fog (coincident with atmospheric warming at shelter height). The relative humidity record indicates that the fog may have initiated in air whose relative humidity without the lake contributions was 65 percent. Figure 14(c), the atmospheric pressure time series, shows additional evidence of cold air advection at the onset of a high-pressure regime.

On the afternoon before the fog the ground had warmed and cold advection was beginning. The acoustic sounder detected strong thermal plumes in the planetary boundary layer (PBL). A set of three-dimensional turbulence data from the wind tower 12-m instruments and the wind speed at the 21-m cup anemometer was recorded as shown in Figure 15(d). The wind speed in meters per second at the 12-m height is shown in Figure 15(a). The corresponding wind direction is shown in Figure 15(b), and the vertical velocity in statute miles per hour is in Figure 15(c). The chart speed was 5.08 cm/min. The turbulence was resolved up to a frequency of approximately 0.5 Hz. There may have been significant vertical turbulence at 2 Hz, and a weighting function to correct for the response of the propeller would have to be determined to permit estimation of 2 Hz turbulence. Also, the chart speed should be increased by at least a factor of five.

It is possible to describe individual turbulent or thermal entities by manual analysis and computation from the strip charts. It is even possible to compute statistical estimates manually for short records. Computations for statistically stationary estimates of means, root mean square fluctuations,

cross and auto correlations (space and time), and frequency spectra are so lengthy as to require use of a digital computer. This implies the need to perform reduction of the chart curves to time series of digital data on punch cards or computer-compatible magnetic tape.

A short segment of the time series of the three-dimensional velocity at the 12-m height has been tabulated manually as digital data. A program to calculate running mean values and turbulence properties has been written and used with the sample data. The resulting values are listed in Table 1. The original velocity data and the computer program are included in Appendix A. The relation between the strength of acoustic echoes and properties of turbulence is discussed in Appendix B.

TABLE 1. THE MEAN AND TURBULENCE PROPERTIES AT 12-m ABOVE THE GROUND IN CLEAR AIR WITH STRONG THERMALS ON THE DAY BEFORE THE FOG (Fig. 15) (TIME INTERVAL 1310 LST TO 1326 LST, 22 MARCH 1977).

Property	Magnitude	Units
\bar{u} , mean zonal wind speed	0.0	m s ⁻¹
\bar{v} , mean meridional wind speed	-6.3	m s ⁻¹
\bar{w} , mean vertical wind speed	0.0	m s ⁻¹
σ_u , rms zonal fluctuation	4.6	m s ⁻¹
σ_v , rms meridional fluctuation	3.7	m s ⁻¹
σ_w , rms vertical fluctuation	0.2	m s ⁻¹
$\rho \overline{u'w'}$, eddy transport of momentum	-0.1	kg m ⁻¹ s ⁻²
$\rho \overline{v'w'}$, eddy transport of momentum	0.2	kg m ⁻¹ s ⁻²
$\rho \overline{u'v'}$, eddy transport of momentum	1.4	kg m ⁻¹ s ⁻²
K_m , momentum mixing coefficient	~0.1	m ² s ⁻¹

Figure 16(d) shows wind data like that in Figure 15(d) except for just after local noon on the day of the fog, 23 March. The thermal plumes which were observed by acoustic radar to be weaker were weaker in measured horizontal and vertical velocity fluctuations. The mean winds were of about the same magnitude at the two different times.

V. THE ISLAND FIELD LABORATORY

A. The Siting of Instruments

The field instrumentation was moved from the UTSI to an island in the lake in the Fall of 1977. By mid-November all equipment except the tower and the transmissometers was operational. The 4-kW electrical generator was in place, and power cables were installed. The location of each instrument system is shown in Figure 17. The instruments were sited on the north-northeast shore to be exposed to the fog airflow having at least a 1 km fetch over water. Advection fogs generally form over the lake in airflow from the northern quadrants. A photographic 200-mm telephoto view from the lake toward the northwest, across the point of the island, is included in Figure 18. The 10-m tower in front on the island appears to the left of the Space Institute, which is on the background shore. Figure 19 presents the island instrument site just a few feet to the left of that portion shown in Figure 18. The hygrothermograph shelter is on the shore, and the shelter for the meteorological tower, electronics, and the tethered-balloon system can be seen through the brush. The balloon system can be seen through the brush. The balloon winch is positioned on the beach next to the operator. A map of the lake and its shoreline is shown in Figure 20. North is to the top of the map. The laboratory at UTSI is marked with an upper case L, and the field site on Elder Island is marked with an F.

B. Shelters

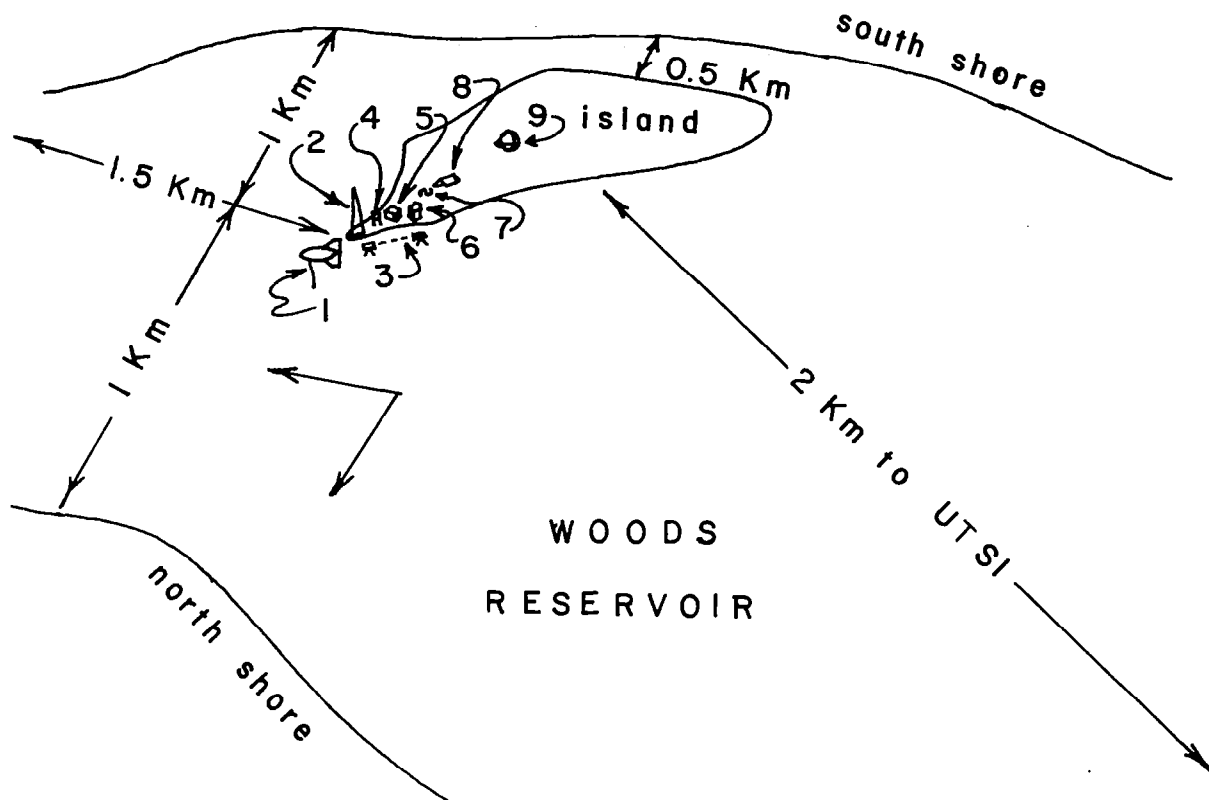
Weather shelters were constructed at three locations to provide protection for (1) the power supply, (2) the electronics, (3) the tether-balloon in storage, and (4) the research workers.

C. Operational Aspects of the Island Site

Transportation of bulky equipment and personnel to the island was by paddled canoe and was difficult, especially on windy days.

The electrical generator required fuel resupplies at frequent intervals. However, the power supplied was quite suitable.

To study the life cycle of a fog it is necessary to keep the island station in operation often for periods of longer than 24 hr, and certainly overnight. It is necessary to have one person on the island at all operation times. It is highly desirable to keep two persons on the island for the following reasons:



Symbol	Description of Equipment
1.	Boundary Layer Profile Balloon
2.	10-m Meteorological Tower
3.	1-m Transmissometer
4.	Hygrothermograph, Microbarograph
5.	Meteor. Tower Recorders
6.	Acoustic Radar-Monostatic
7.	4-kW, 60-Hz Electrical Generator
8.	Acoustic Radar Instrumentation
9.	Acoustic Radar-Bistatic Antenna

Figure 17. An oblique drawing of the island and instrumentation setup.
 (The location of each piece of apparatus, as of 18 November 1977, is shown by symbols defined in the legend.)



Figure 18. A telephotographic view (toward the northwest) of the island site (on the left) and the University of Tennessee Space Institute across the lake (on the right).



Figure 19. A close telephotographic view of some of the instrumentation and shelters on the island.

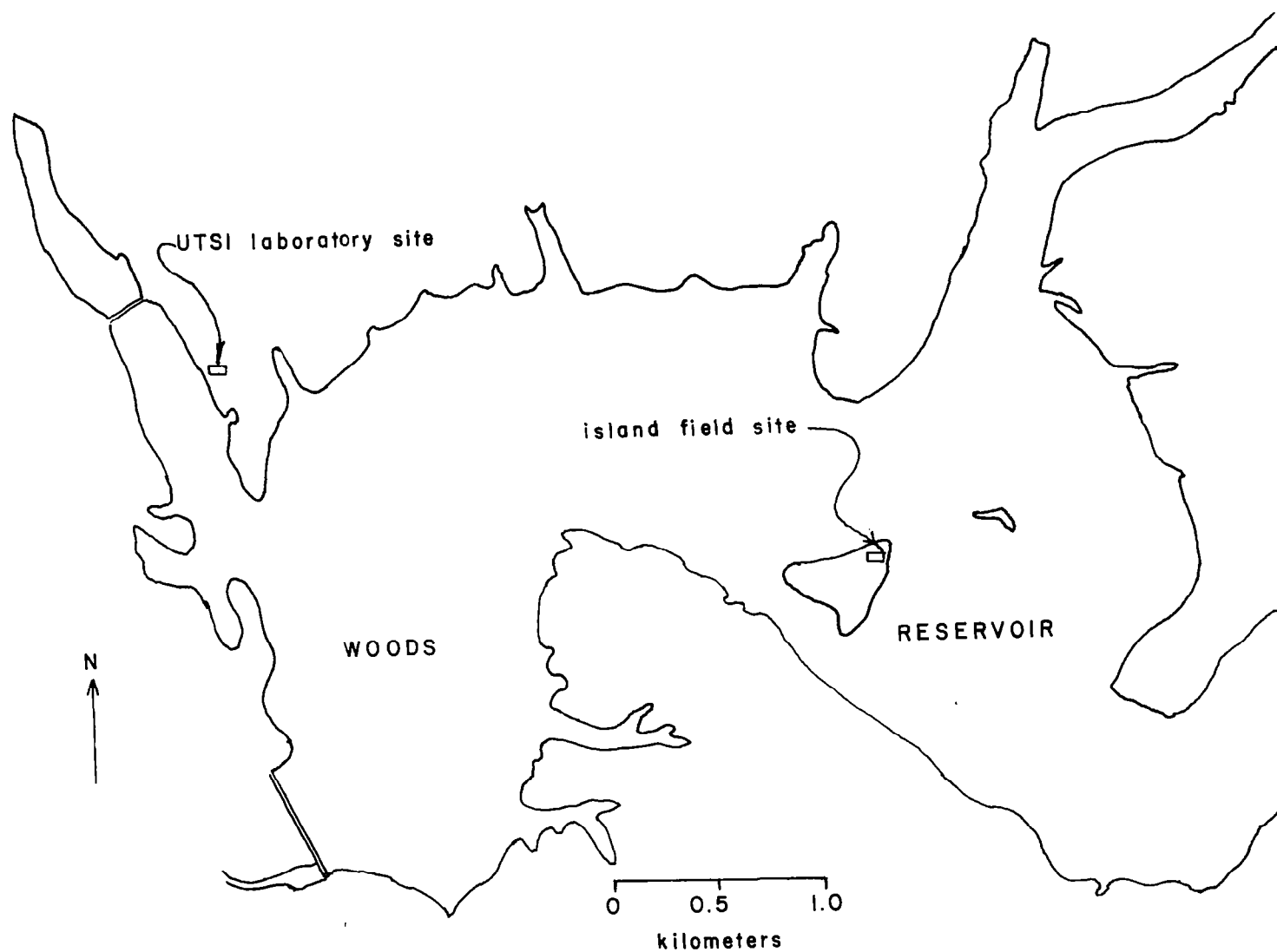


Figure 20. An outline map of the lake, the island field site, and the UTSI laboratory site.

- 1) Many measurements and instruments are involved.
- 2) There are some potential hazards, especially in a night and wet environment at a remote island site.
- 3) A backup person should be available to keep the operation going when problems arise.

It is necessary to relieve the personnel on the island at intervals of 5 to 8 hr.

In summary, it has been demonstrated that a program of measurements of fog airflow properties spanning the life cycle of a fog at a remote lake site now can be executed. The number of case studies which can be accomplished is limited primarily by availability of personnel and logistic support.

Section VI describes the first fog study performed on the island over a period of approximately 24 hr. The preliminary results are presented, and recommendations for improving the program are made.

VI. A FOG CASE STUDY AT THE REMOTE LAKE SITE

On the afternoon of 22 November 1977, cold air advection began and fog formed in the region around and over Woods Reservoir. (On the previous evening a fog similarly "rolled into the area." A field operation was initiated, but that fog did not persist for more than 2 hr.) By late afternoon it was apparent that the second fog would persist, and the island site was activated. Three graduate students and the principal investigator shared the measurement and logistic duties for the next 24 hr.

The acoustic radar was functional part of the time. The hygrothermograph and microbarograph were operational. The tethered-balloon boundary layer profiles was at least partially functional, although the wet condition caused some electronic problems with the multiplexing circuit, the thermometer circuits, and the winch controller. The majority of the soundings were accomplished by using the following two expedients:

- 1) The balloon and instruments were raised and lowered by hand-over-hand deployment of the tether line when the winch failed.

2) The sensor-multiplex-telemeter package was weatherproofed by conditioning with a hair dryer airstream and then enclosing all but the sensors in a large baggy.

The acoustic sounder record is shown in Figure 21. The quality is much below standard and relates to instrument adjustment and degradation during the experiment period as well as inadequate training of personnel. Nevertheless, the structure of the echo can be seen. The data show that the acoustic beam of the current antenna is very wide, making noise reception rather large and signal-to-noise ratio smaller than can be achieved.

Figure 22 contains the plots of vertical distributions of (a) temperature, (b) wet-bulb temperature, (c) wind speed, and (d) direction, as measured at different times during the study. The time series of profiles indicates considerable variation in conditions. The validity of some temperature data is still in question. An effort will be made in the next few months to evaluate this preliminary data.

Surface values of meteorological variables at the island are plotted as a function of time in Figure 23. The transmissometer data curve (e) remains questionable, but its indication of less fog coincides with a decrease in relative humidity as measured by a hygrothermograph (plotted as curve d).

VII. CONCLUSIONS

A. Interpretation of the Measurements

The case study of fog in the land site at UTSI indicated that two physical phenomena may have triggered the onset and maintenance of lake fog by cold air advection:

1) A small acoustic echo region appeared and descended to continually lower heights above the main inversion.

2) The turbulence intensity as measured by half peak-to-peak values became smaller than the already low magnitude of the mean wind.

These phenomena need to be understood and documented more thoroughly by obtaining more case studies.

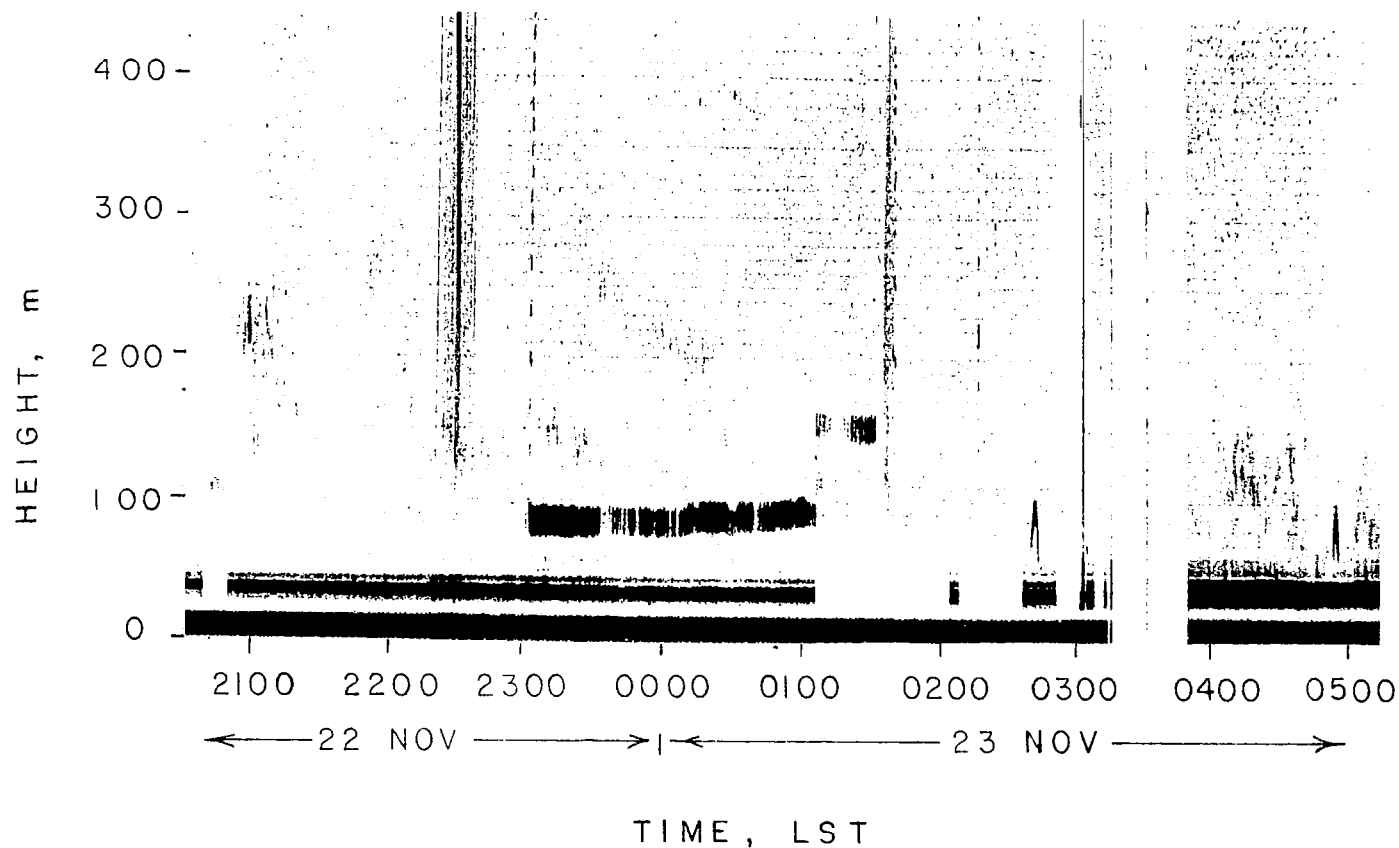


Figure 21a. Sample acoustic radar record taken at the island site during fog. (Time 2100 LST 22 November to 0500 LST 23 November 1977. The strong echo band aloft is from a balloon. Several other artifacts show on the record.)

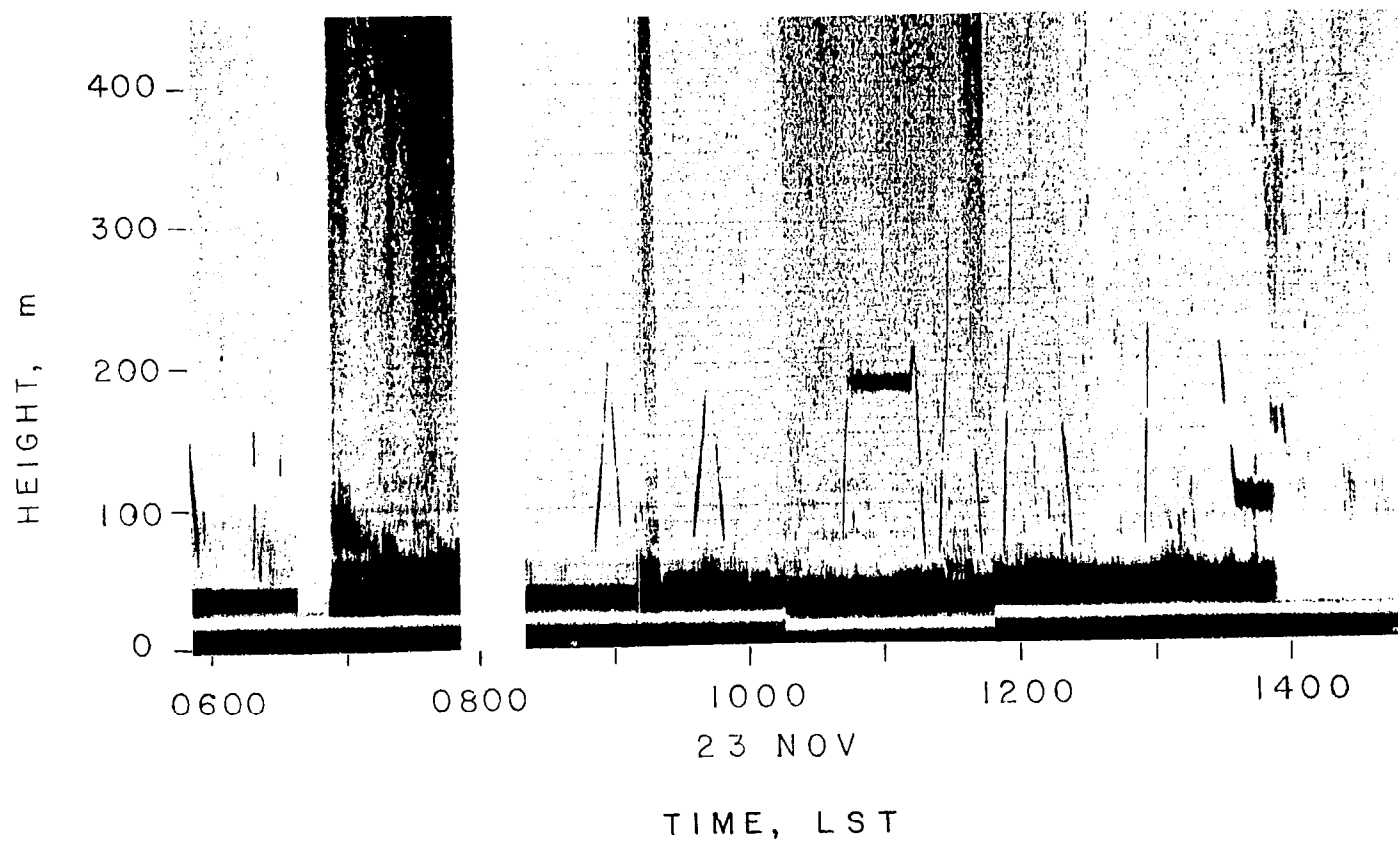


Figure 21b. Continuation of sample acoustic radar record taken at the island site after fog had dissipated on 23 November 1977.

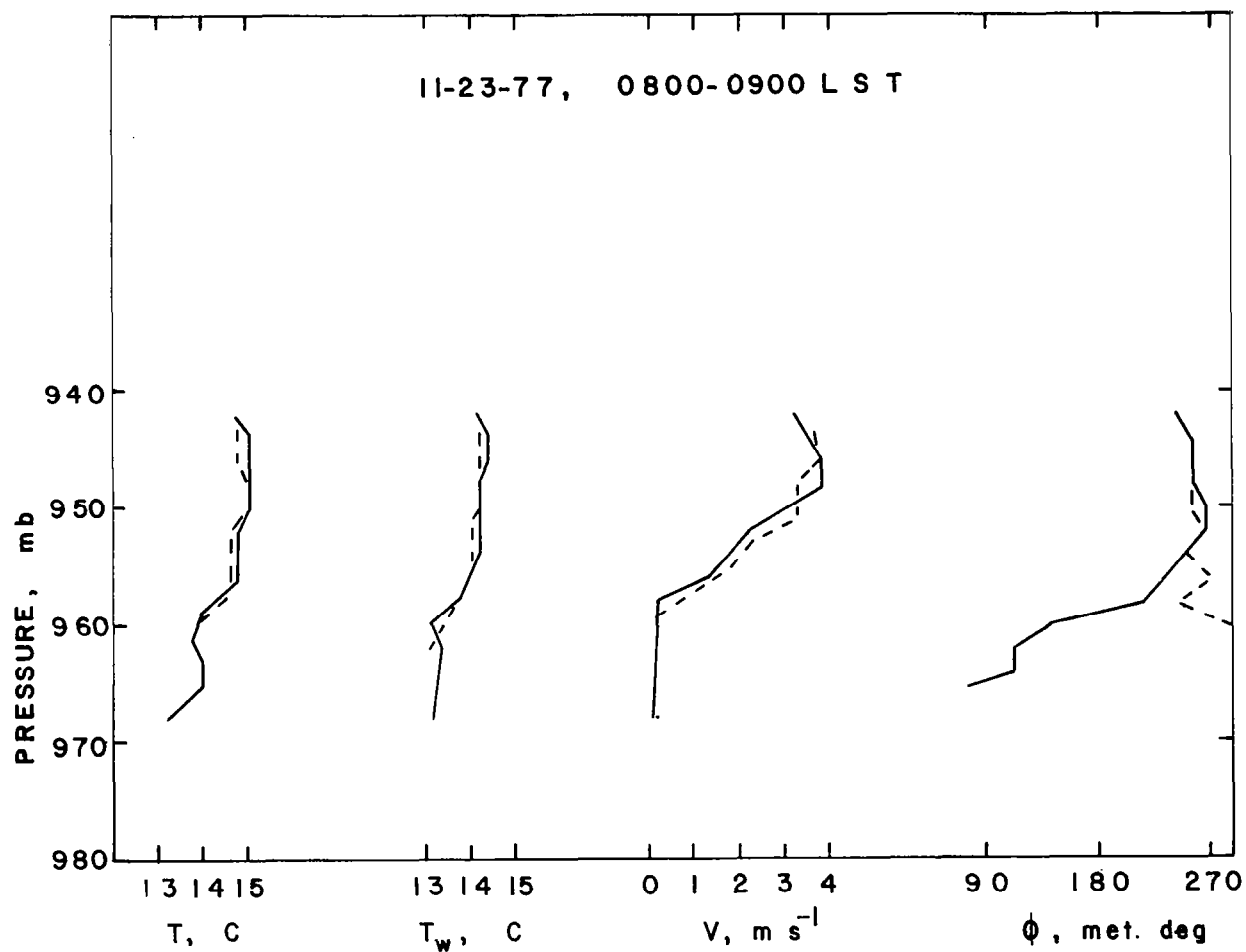
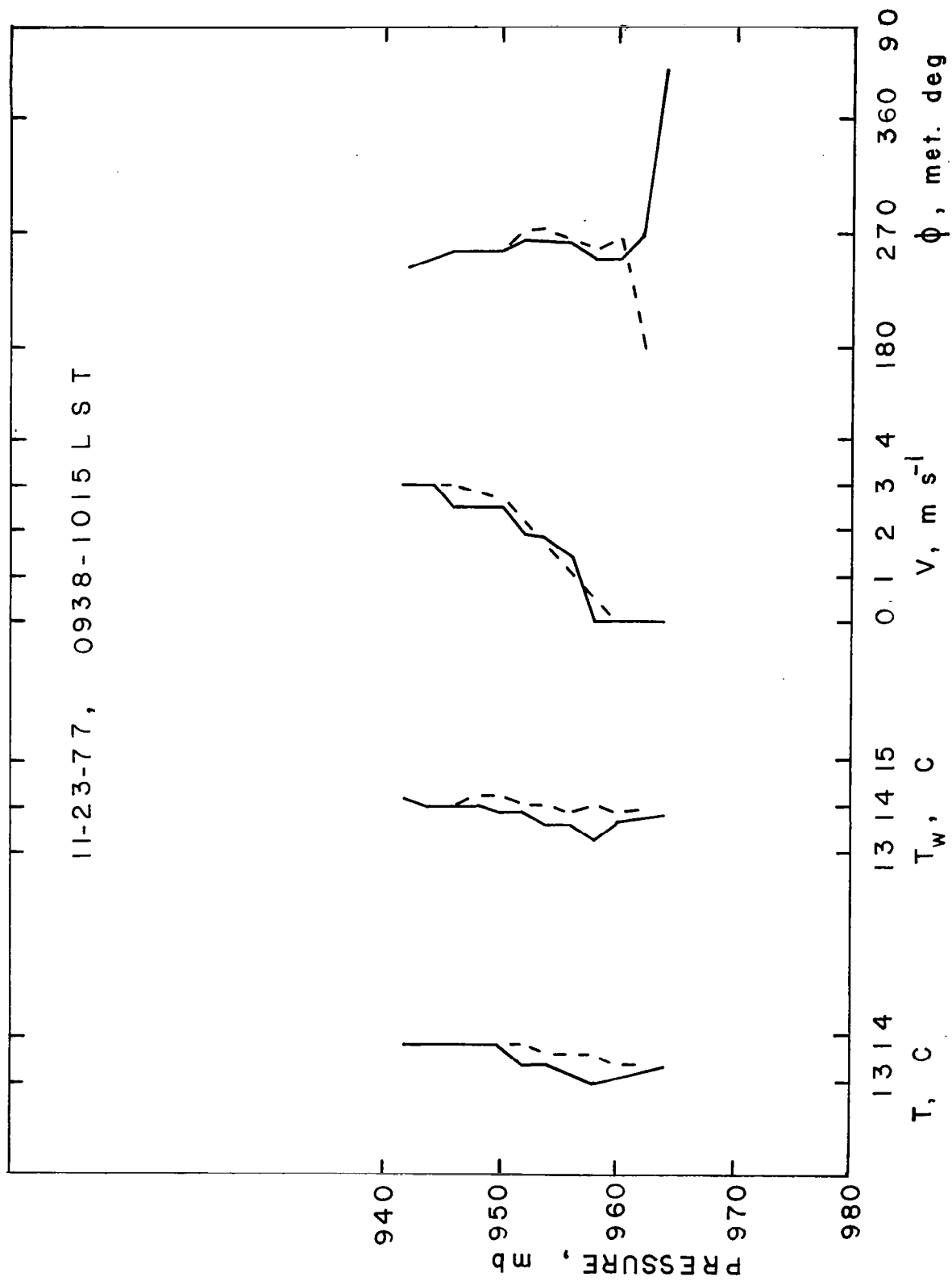


Figure 22. Sample vertical distributions of atmospheric boundary layer temperature, wet-bulb, temperature, horizontal wind speed, and horizontal wind direction measured from a tethered-balloon boundary layer profiler. (The solid lines are for the ascent, and the dashed lines are for the descent portion of the sounding. Time: November 23, 1977, 0800 to 0900 LST.)



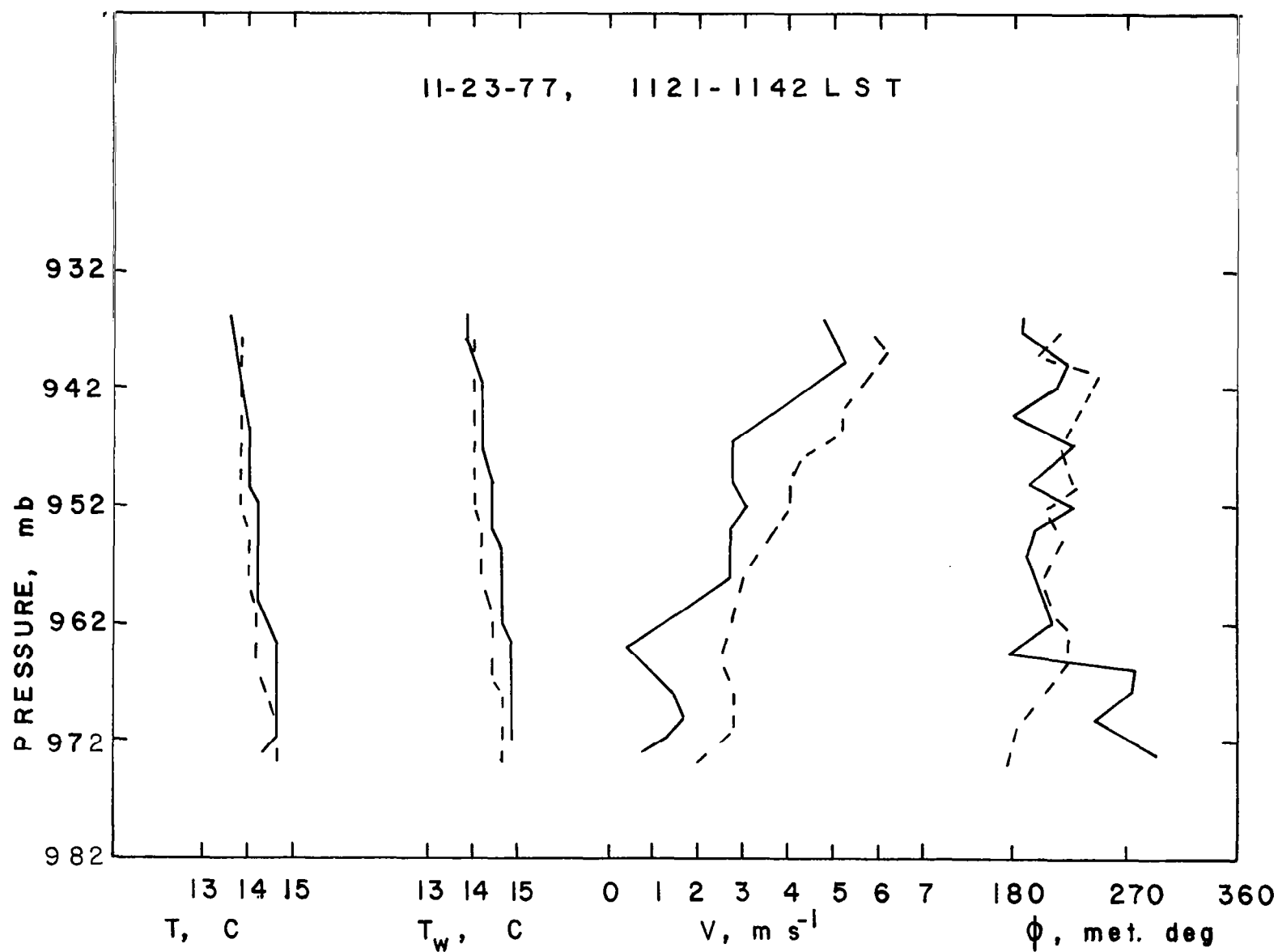


Figure 22. (Continued)

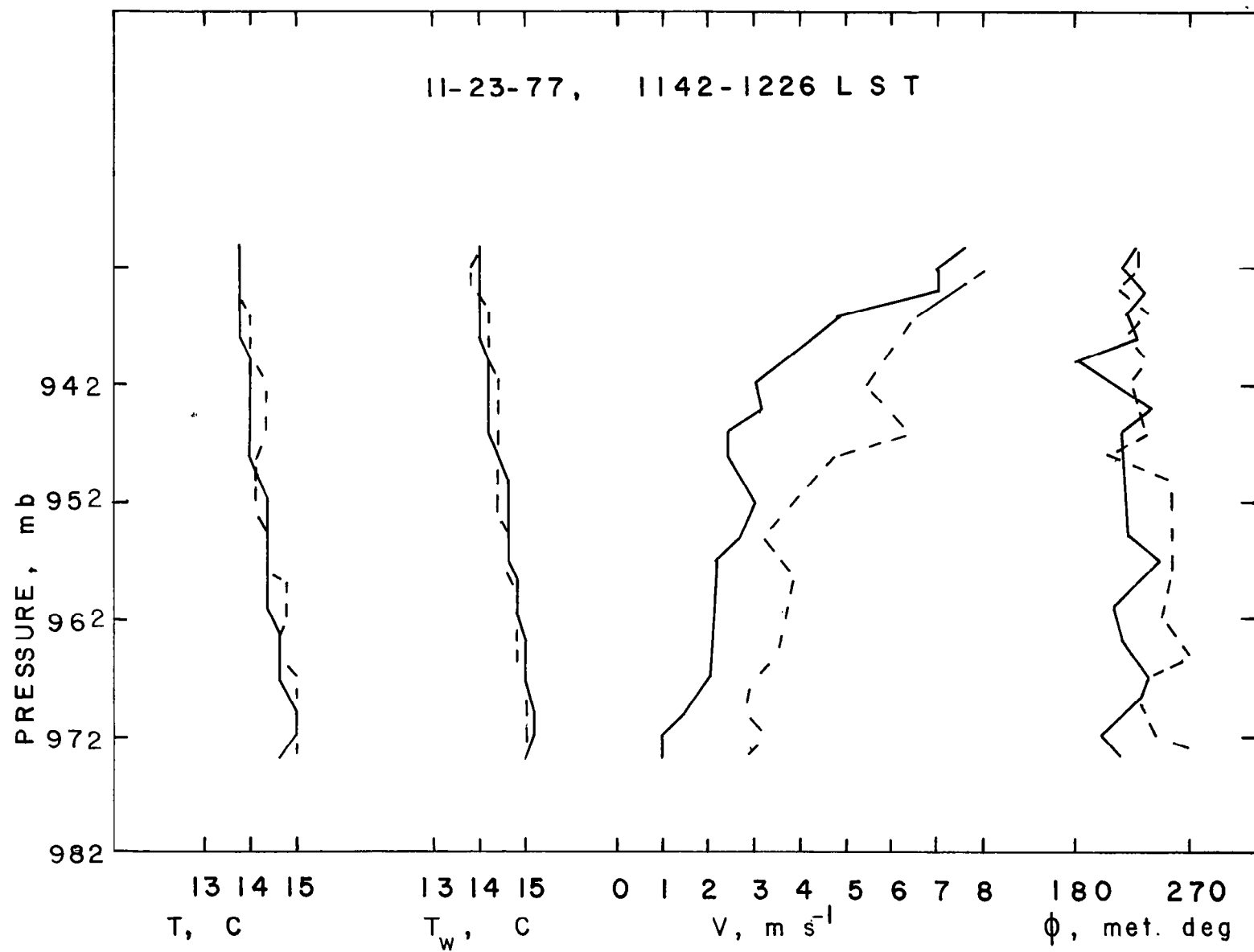


Figure 22. (Continued)

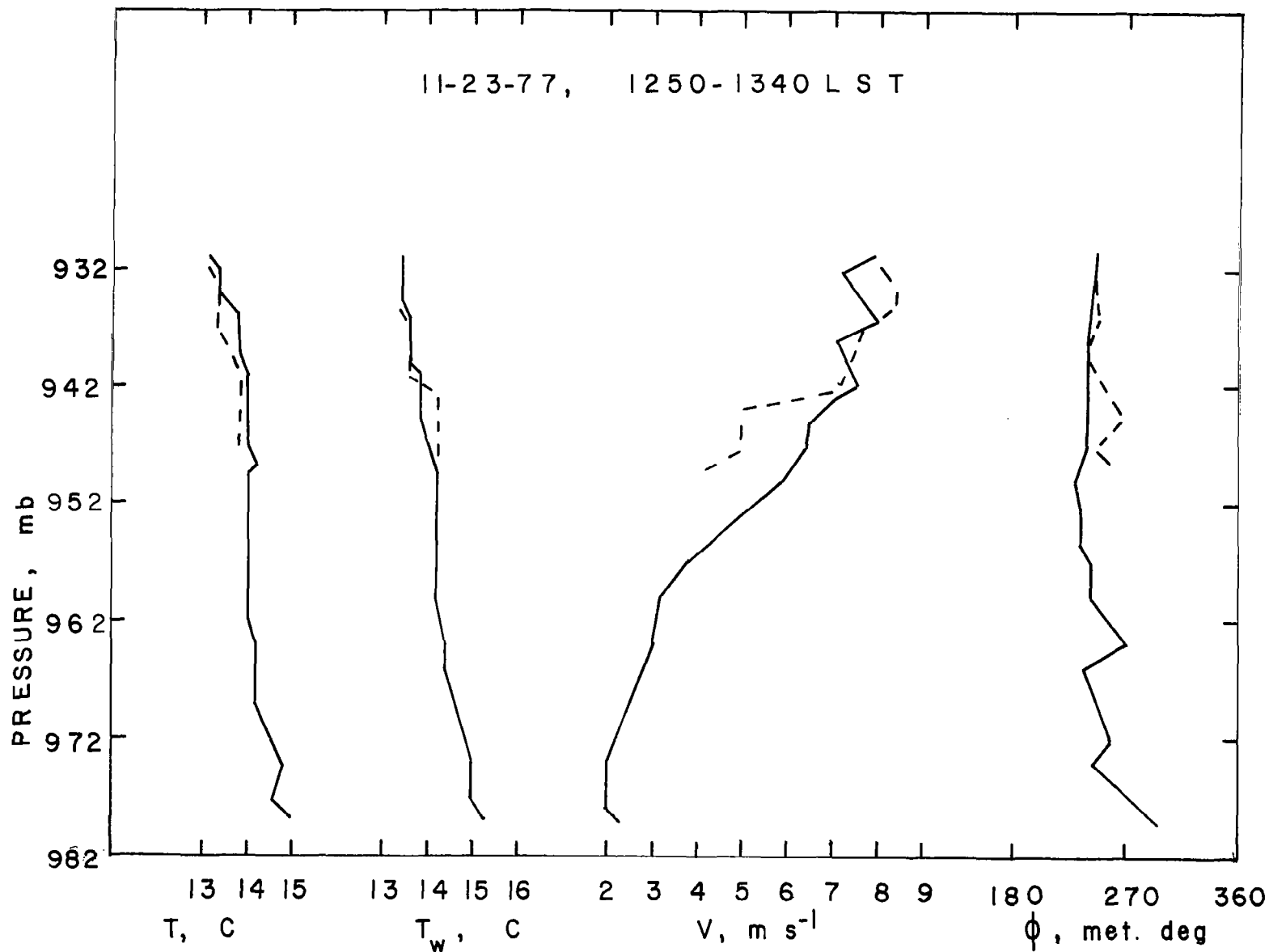


Figure 22. (Concluded)

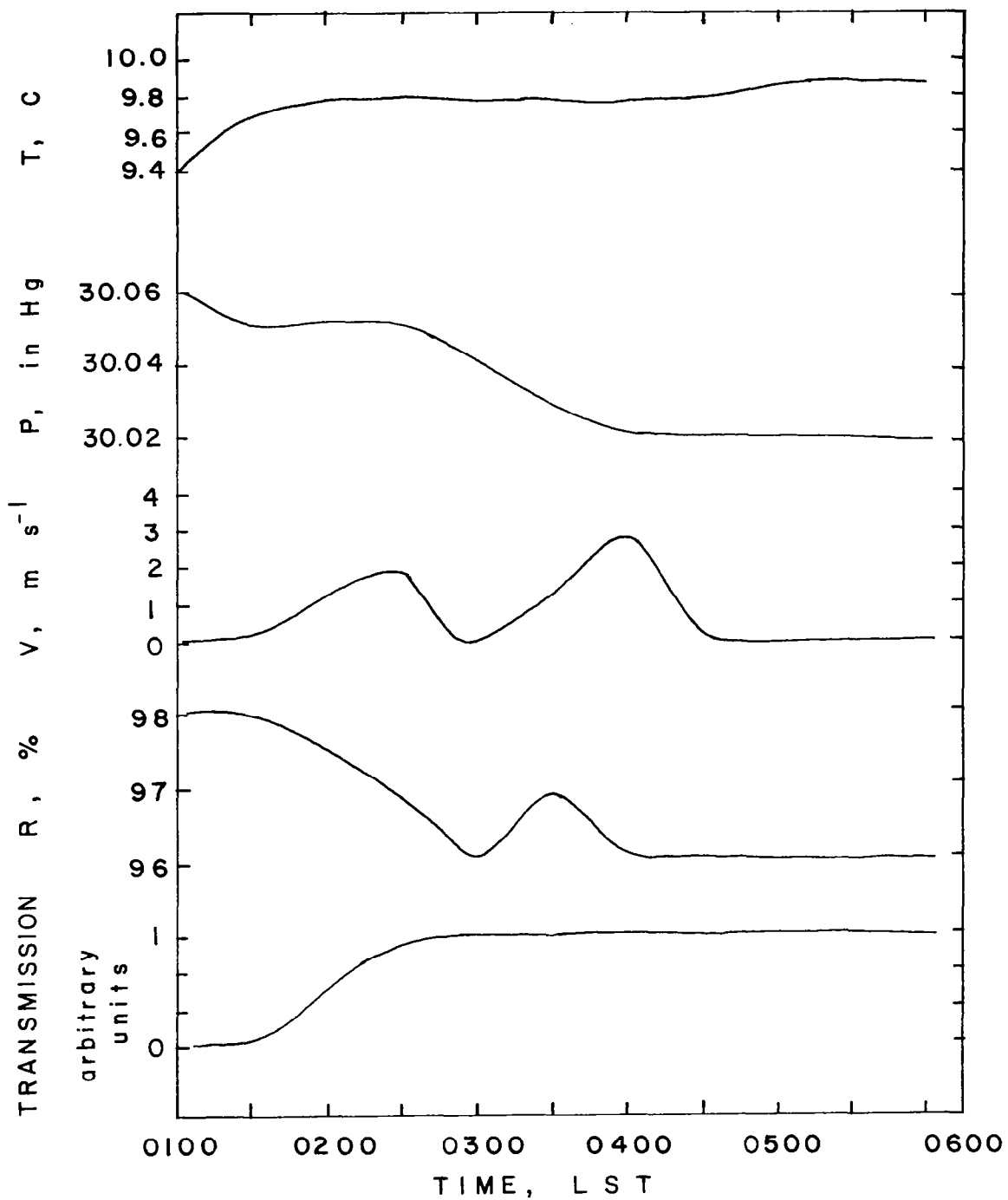


Figure 23. Smoothed graphs of atmospheric variables at the surface at the island site during the time interval which includes the dissipation of a fog. The variables plotted are, from top to bottom: temperature, static pressure, horizontal wind speed, relative humidity, and fraction of transmission of a light beam through the air to a light detector.

The acoustic sounder records from the lake site indicate a much lower and simpler inversion structure and also less thermal activity in the boundary layer. It is not certain how much of this difference is due to difference between land and water and how much is due to seasonal differences.

Horizontal gradients of lake temperature or shore breezes, or both, can strongly affect fog over the lake. Figure 24 shows fog viewed to the northwest from the lake on the west side of the island. The fog covered the land on the north side of the lake and the lake as far as the middle region, where the fog bank remained relatively stationary.

B. Recommendations

In the next year or so a set of case studies should be assembled from new measurements over water.

A tethered balloon system appears useful to describe some aspects of temperature and wind through the full thickness of the fog layer. A considerable improvement would be achieved by use of a Doppler acoustic sounder at approximately three times the cost of purchasing the balloon system. At present neither the balloon system nor the Doppler acoustic sounder have been purchased.

The site instrumentation should be set up more functionally on the island and a series of nonfog and fog case studies performed in the next half year to improve the field measurement capability.

A second acoustic radar operated concurrently at a land site on the north side of the lake could permit characterization of changes in the fog turbulence which is due to the lake environment.

Numerical models of fog and direct measurements of turbulence in fog should be compared with a model of fog related to acoustic radar measurements. Specifically, the results of each numerical model of fog should be used to calculate the corresponding acoustic radar echo intensity distribution, and the results will be compared with real acoustic radar records of the same type. The comparison then could be used to derive requirements for making improved numerical models of fog.

fog top (50 m)

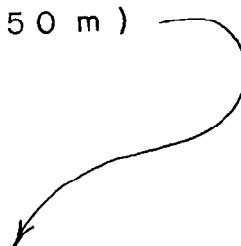


Figure 24. A fog bank northwest of the island site. The fog was formed by cold advection and the slightly buoyant elements.

APPENDIX A

DIGITAL COMPUTATION OF THE TURBULENCE PROPERTIES OF THE THREE-DIMENSIONAL AIRFLOW MEASURED WITH A METEOROLOGICAL TOWER

The computer program in this appendix is for the calculation of mean values, root mean square values of the fluctuations, and cross correlations of the three orthogonal components of wind velocity. Such calculations will permit independent measurement of significant variables put into numerical models of fog. At present the data are read into the program from data cards punched by hand and read by eye from analog graphs of velocity components.

A crude analog-to-digital conversion system will be constructed in the near future to permit turbulence computations using a necessarily larger amount of data.

```

0001      PARAMETER N=351
0002      DIMENSION IVH(N),ITH(N),IWW(N)
0003      DIMENSION U(N),V(N),W(N)
0004      CALL ASSIGN(1,'SY:F.DAT')
0005      CALL ASSIGN(2,'F.OUT')
0006      SUMU=0
0007      SUMV=0
0008      SUMW=0
0009      IS=1
0010      IE=8
0011  10  READ (1,101) ((IVH(I),ITH(I),IWW(I)),I=IS,IE)
0012  101  FORMAT (8(I3,I3,I4))
0013      DO 100 I=IS,IE
0014      V(I)=0.1*IVH(I)*SIN(0.0175*ITH(I)-1.57)
0015      U(I)=0.1*IVH(I)*COS(0.0175*ITH(I)+1.57)
0016      W(I)=0.01*IWW(I)*0.447
0017      SUMU=SUMU+U(I)
0018      SUMV=SUMV+V(I)
0019      SUMW=SUMW+W(I)
0020  100  CONTINUE
0021      IS=IS+8
0022      IE=IE+8
0023      IF (IS.LT.N) GO TO 10
0024      UM=SUMU/N
0025      VM=SUMV/N
0026      WM=SUMW/N
0027      SUMU=0
0028      SUMV=0
0029      SUMW=0
0030      SUMVU=0
0031      SUMVW=0
0032      SUMUW=0
0033      DO 200 I=1,N
0034      SUMU=SUMU+(U(I)-UM)**2
0035      SUMV=SUMV+(V(I)-VM)**2
0036      SUMW=SUMW+(W(I)-WM)**2
0037      SUMVU=SUMVU+(V(I)-VM)*(U(I)-UM)
0038      SUMVW=SUMVW+(V(I)-VM)*(W(I)-WM)
0039      SUMUW=SUMUW+(U(I)-UM)*(W(I)-WM)
0040  200  CONTINUE
0041      SUMH=(SUMU+SUMV)
0042      STDV=SQRT(SUMV/N)
0043      STDU=SQRT(SUMU/N)
0044      STDW=SQRT(SUMW/N)
0045      STDH=SQRT(SUMH/N)
0046      VUM=SUMVU/N
0047      VWM=SUMVW/N
0048      UWM=SUMUW/N
0049      WRITE(2,201) UM,VM,WM,STDV,STDU,STDW,STDH,VUM,VWM,UWM,
0050  201  FORMAT (11(1,2X,'UM=',F7.2,1X,'M./S.',/,2X,'VM=',F7.2,1X,'M./S.',
1/,2X,'WM=',F7.2,1X,'M./S.',/,2X,'STDV=',F7.2,1X,'M.S.',/,2X,'STDU='
1,F7.2,1X,'M./S.',/,2X,'STDW=',F7.2,1X,'M./S.',/,2X,'STDH=',F7.2,1X
1,'M./S.',/,2X,'VUM=',F7.2,1X,'M**2/S**2',/,2X,'VWM=',1X,F7.2,1X,
1'M**2/S**2',/,2X,'UWM=',F7.2,1X,'M**2/S**2')
0051      STOP
0052      END

```


APPENDIX B

THE RELATION BETWEEN THE STRENGTH OF ACOUSTIC ECHOES AND PROPERTIES OF TURBULENCE

Tatarski¹ derived a relation between the acoustic power scattered by air creating fluctuations of the speed of sound, c , by thermal and speed fluctuations of the air. He assumed the Kolmogorov spectrum of turbulence and obtained the following relation:

$$P_s = 0.03k^{1/3} \cos^2 \theta \left[\left(\frac{C_v^2}{c^2} \right) \cos^2 \left(\frac{\theta}{2} \right) + 0.13 \left(\frac{C_T^2}{T^2} \right) \right] \left(\sin \frac{\theta}{2} \right)^{-1/3}$$

where

P_s = the scattered power per unit volume per unit incident flux per unit solid angle

k = the wave number of the incident acoustic signal

θ = the angle from forward propagation of the scattered signal

c = the speed of sound

T = the absolute temperature

C_v = the velocity structure coefficient

C_T = the temperature structure coefficient.

The structure coefficients are defined as follows:

$$C_v^2 \equiv \frac{\overline{(W'(x) - W'(x+R))^2}}{R^{2/3}}$$

-
1. Tatarski, V. I., Wave Propagation in a Turbulent Medium. New York: Dover Publications, 1961.

$$C_T^2 \equiv \frac{\overline{(T'(x) - T'(x+R))^2}}{R^{2/3}}$$

where

W' = the speed of fluctuation of the wind

T' = the fluctuation of temperature

R = the radius vector length of one position in the air

x = the separation of a second parcel of air from the first.

Little² showed that the power returned is given for monostatic operation, $\theta = 180^\circ$, as

$$P_r = P_s \sigma h A_r \frac{L}{R^2}$$

where

P_s = scattered acoustic power

σ = scattering cross section

h = pulse half-width

A_r = normal area of the receiving antenna

L = total attenuation factor

R = range from transmitter to scattering element.

-
2. Little, C. G., On the Detectability of Fog, Cloud Rain and Snow by Acoustic Echo-Sounding Methods. J. Atmospheric Science, 29, 748-758, 1972.

The last relation may be written in terms of C_T (and C_v in the more general case). If the turbulence properties are specified or calculated as they would be for a numerical model of an advection fog, C_T and C_v may be calculated. Thus P_r becomes a function of variables whose values are specified or calculated. The appropriate form of this relation will be derived during the next reporting period.

1. REPORT NO. NASA CR-3095	2. GOVERNMENT ACCESSION NO.	3. RECIPIENT'S CATALOG NO.	
4. TITLE AND SUBTITLE A Field Study of Air Flow and Turbulent Features of Advection Fog		5. REPORT DATE January 1979	
		6. PERFORMING ORGANIZATION CODE	
7. AUTHOR(S) J. D. Connell		8. PERFORMING ORGANIZATION REPORT #	
9. PERFORMING ORGANIZATION NAME AND ADDRESS University of Tennessee Space Institute Tullahoma, Tennessee		10. WORK UNIT NO. M-279	
		11. CONTRACT OR GRANT NO. NAS8-32031	
12. SPONSORING AGENCY NAME AND ADDRESS National Aeronautics and Space Administration Washington, D.C. 20546		13. TYPE OF REPORT & PERIOD COVERED Contractor	
		14. SPONSORING AGENCY CODE	
15. SUPPLEMENTARY NOTES Prepared under the technical monitorship of the Atmospheric Sciences Division, Space Sciences Laboratory, NASA/Marshall Space Flight Center			
16. ABSTRACT This report describes the setup and initial operation of a set of specialized meteorological data collection hardware to study the life cycle of advection fogs at a lake test site. A primary goal in the research program was to identify turbulence levels in the fogs and to correlate these data with the temperature gradients and mean wind profiles. An acoustic radar was one of the primary instruments used to collect data for this research. A meteorological tower was instrumented to allow multiple-level measurements of wind and temperature on a continuous basis. Additional instrumentation was: (1) hydrothermograph, (2) microbarograph, (3) transmissometers, and (4) a boundary layer profiler. Two types of fogs were identified, and important differences in the turbulence scales were noted.			
17. KEY WORDS Advection Fog Studies Temperature Turbulence		18. DISTRIBUTION STATEMENT Category 47	
19. SECURITY CLASSIF. (of this report) Unclassified	20. SECURITY CLASSIF. (of this page) Unclassified	21. NO. OF PAGES 50	22. PRICE \$4.50